Molecular Simulation of Porous Coordination Network Based Mixed Matrix Membranes for Flue Gas Separation

by

Çiğdem Altıntaş

A Thesis Submitted to the
Graduate School of Sicences and Engineering
in Partial Fulfillment of the Requirements for
the Degree of

Master of Science
in
Chemical and Biological Engineering

Koc University
August 2015

Koc University

Graduate School of Sciences and Engineering

This is to certify that I have examined this copy of a master's thesis by

Çiğdem Altıntaş

and have found that it is complete and satisfactory in all respects,
and that any and all revisions required by the final
examining committee have been made.

Committee Members:

_____

Seda Keskin Avcı, Ph. D. (Advisor)

_____

Özlem Keskin Özkaya, Ph. D.

_____

Sezen Soyer Uzun, Ph. D.

Date: _____

ABSTRACT

In this thesis, the challenge of selecting porous coordination networks (PCNs) as filler particles in mixed matrix membranes (MMMs) was examined using molecular simulations. PCNs are promising nanoporous materials in gas separations because of their tunable pore sizes, high porosities, good thermal and mechanical stabilities. Gas permeability and selectivity of 200 new MMMs composed of 20 different PCNs and 10 different polymers were calculated for CO_2/N_2 separation. We showed that selecting the appropriate PCN as filler particles in polymers results in MMMs that have high CO_2/N_2 selectivities and high CO_2 permeabilities compared to pure polymer membranes. Several PCN/polymer MMMs were identified to exceed the upper bound established for CO_2/N_2 separation. Effect of framework flexibility of PCNs on the performance of MMMs was also examined. Results showed that considering flexibility of PCNs is important for predicting gas permeability of pure PCNs but has less significance for predicting gas permeability of PCN-filled MMMs whenever the PCN volume fraction is low. For rapid screening of PCN/polymer MMMs, flexibility of the fillers can be neglected as a reasonable approximation if the filler volume fraction is less than 0.3. The methods introduced in this thesis will create many opportunities for selecting PCN/polymer combinations for MMMs with useful properties in CO_2 separation applications.

ÖZET

Bu tezde bir çeşit metal organik yapılı malzeme olan gözenekli koordinasyon ağlarının (PCN) karışık yataklı membranlarda (MMM) dolgu olarak kullanılması moleküler modelleme yöntemiyle incelenmiştir. PCNler ayarlanabilir gözenek boyutları, yüksek gözenek hacimleri ve iyi ısıl ve mekanik dayanıklılıkları sebebiyle gaz ayırma işlemleri için umut verici nanogözenekli malzemeler olarak değerlendirilmektedir. Bu tezde 20 farklı PCN ve 10 farklı polimer ile hazırlanmış 200 PCN-dolgulu MMMnin gaz geçirgenlik ve seçicilikleri CO_2/N_2 ayırımı için hesaplanmıştır. Uygun PCNler dolgu olarak seçildiği takdirde oluşturulan MMMlerin saf polimerlere göre daha yüksek geçirgenlik ve seçiciliğe sahip olabileceği ispatlanmış ve hatta bu şekilde oluşturulan PCN/polimer çiftlerinin bir kısmının Robeson tarafından CO_2/N_2 ayırımı için belirlenen üst sınırı geçebileceği gösterilmiştir. Tezin bunu izleyen kısmında PCNlerin esnekliğinin MMM performansına etkisi varsayımsal olarak incelenmiştir. Bu çalışma PCN esnekliğini dikkate almanın PCNnin gaz geçirgenliğine önemli bir etkisi olduğunu ama özellikle PCNnin hacimsel oranının düşük olduğu PCN-dolgulu MMMlerin gaz geçirgenliğine daha az etkisi olduğunu göstermiştir. Buna dayanarak PCN/polimer MMMlerinin performanslarının hızlıca taranabilmesi için PCNnin membran içindeki hacimsel oranının 0,3'ün altında olduğu durumda PCN esnekliğini dikkate almamanın uygun olacağına karar verilmiştir. Bu tezde tanıtılan yöntemler CO_2'yi diğer baca gazlarından ayırmak için seçilecek kullanışlı PCN-dolgulu polimer membranların belirlenmesinde birçok fırsat sunmaktadır.

ACKNOWLEDGEMENTS

I want to primarily thank to my advisor, Assoc. Prof. Dr. Seda Keskin who has trusted and always been patient with me from the first day. I know that with accepting my application for graduate study that day, Dr. Keskin has given me a valuable opportunity with which I hope to move forward to contribute accurate and useful information to scientific knowledge. This opportunity also made it possible for me to know the beautiful people in her group, NEMO.

The feeling of safety because of their sincerity has always been what is in common. İlknur is the goodwill and determination delegate of NEMO. She is one of the super duper people I know and I feel very grateful and happy to know her and to be her friend. With Tuğba in the office, on almost every day I remember us laughing at a word or move of her. The care she provides for her work and the peacefulness she emits during studying has always made me feel a desire to go to my desk and study with peace like her. Aydın has always generously shared his valuable knowledge in every area, and he made me aware of that I should always feel responsible for the development of first myself and then also of the people around me. Elda, the lovely and funny new member of NEMO, has brought a beautiful enthusiasm to our group. I have learned many from Elda and I hope we will continue to learn from each other.

I want to express my sincere thanks for the people in the GSSE office, Elif Hanım, Emine Hanım and Gözde, as they always make this faculty feel like a home and I want to thank Songül abla, Ayşe abla, Hacer abla, Ümmü abla and Türkan as they are a valuable part of this home. I had the luck to have Gamze and Kardelen as irreplaceable friends during both the graduate and undergraduate years of us. I want to thank to them in advance for all the care and love they shared with me until now and in the future.

Although from now on we are going through different routes, our good wishes for each other are always with us.

I want to thank Selin, Nur Sena and Seçil for their understanding for all the times I could not find time to be next to them. I hope we will compensate these in the future while we keep learning, growing up and being strong with each other.

I will always long for the peaceful home of Ozbecidar as it is the place I had two of the most beautiful, cheerful, peaceful, thoughtful and warmhearted years of my life. I am sure it is the same for all the special people of Ozbecidar. Sometimes I feel surprised when I see how lucky we are to have each other. As it was not good enough to have each other, I met many valuable people thanks to them. I hope we continue to become a bigger family of beautiful people with time.

For teaching and supporting me to stand on my own feet and making all of these possible, I want to thank to my mother, my father and my sister. All of these would not be possible if my mother was not such a powerful mother with pure joy of living, my father was not such a thoughtful father with his foresight full of wisdom and my sister was not such a super sister full of talent and empathy.

As it is said, the bond that linked my true family was not one of blood, but of respect and joy in each other's life.

Last but not the least; I want to thank to my thesis committee members Prof. Dr. Özlem Keskin Özkaya and Asst. Prof. Dr. Sezen Soyer Uzun for accepting to be in my thesis committee and for their supportive comments. Financial support provided by The Scientific and Technological Research Council of Turkey (TUBITAK) Grant MAG-213M401 is gratefully acknowledged.

Çiğdem Altıntaş

28 August 2015

TABLE OF CONTENTS

LIST OF TABLES

LIST OF FIGURES

NOMENCLATURE

CO_2	: Carbon dioxide
O_2	: Oxygen
N_2	: Nitrogen
NO_x	: Mono-nitrogen oxide
SO_x	: Sulfur oxide
MMM	: Mixed matrix membrane
MOF	: Metal organic framework
ZIF	: Zeolite Imidazolate Framework
PCN	: Porous Coordination Network
GCMC	:Grand Canonical Monte Carlo
EMD	: Equilibrium Molecular Dynamics
IRMOF	: Isoreticular MOF
PDMS	: Polydimethylsiloxane
XLPEO	: Cross-linked polyethylene oxide
PI	: Polyimide
PVAc	: Polyvinyl acetate
ODA	: Oxydianiline
PIM	: Polymers of intrinsic microporosity
PTMGP	: Polytrimethylgermylpropyne
PTMSP	: Polytrimethylsilylpropyne
U	:Potential energy
ε_0	: Dielectric constant
r	: Position of atom
D_0	: Corrected diffusivity
D_t	: Transport diffusivity
c	: Adsorbed gas amount
f	:Bulk phase fugacity
∇c	:Concentration gradient
J	:Gas flux
P_f	:Filler's permeability
ΔP	:Pressure drop
L	:Membrane thickness
S	: Ideal selectivity
BET	:Braunet-Emmett-Teller
S_{acc}	:Accessible surface area
V_{pore}	:Pore volume
LPD	:Limiting pore diameter
LCD	:Largest cavity diameter
ϕ	:Volume fraction of filler in polymer matrix
P	:MMM's gas permeability
P_p	:Polymer's permeability

ε	:Potential well depth
σ	:Potential diameter
q	:Partial charge
λ_{fp}	:Ratio of filler's permeability to polymer's permeability
P_{eff}	:Effective permeability
β^{*}	:Matrix rigidification factor
ϕ_S	:Volume fraction of the dispersed phase
ϕ_I	:Volume fraction of the interphase
AARE	:Average absolute relative error
UFF	: Universal Force Field
OPLS-AA	:Optimized potential for liquid simulations all-atom
EQeq	:Extended charge equilibriation method
CBAC	:Connectivity-based atom contribution
REPEAT	:Repeating electrostatic potential extracted atomic charges
DDEC	:Density-derived electrostatic and chemical charges
NVT	:Constant number of molecules, volume and temperature

Chapter 1

INTRODUCTION

Rising levels of CO_2 in the atmosphere behave as a trap for heat reflecting back from the earth's surface. This trap causes warming of the globe which as a result changes the living conditions of the species of earth in an increasing rate that species cannot easily adapt to. A relatively short term precaution to avoid higher levels of CO_2 in the atmosphere is the capture and sequestration of CO_2; however the separation and capture of CO_2 from its gaseous mixtures require highly costly processes. Therefore, it is urgent to understand and manage the sources of CO_2 emissions to the atmosphere and slow down the rate of its delivery [1]. Flue gas is a mixture composed mainly of water-saturated N_2 with smaller amounts of CO_2, O_2 and other species. Since significant amount of gaseous CO_2 emitted to the atmosphere is due to the flue gas emission from fossil fuel power plants, cost-effective technologies for capturing CO_2 from flue gas are of great importance. It is desired to achieve this separation efficiently, with low cost and low energy requirements under acceptable operating conditions. Several methods have been already developed to accomplish this including absorption, adsorption, cryogenic distillation and membrane separation.

Absorption utilizes the difference of chemical affinity of a solvent to the components of the flue gas and can separate flue gas mixtures with high purity, more than 95% [2]. If the solvent has a strong attraction for CO_2, regeneration requires a more effortful process, but when the solvent has low attraction for CO_2, regeneration of the solvent becomes easier while the purity of the separated stream becomes lower. This trade-off between the level of attraction of the solvent to CO_2 and ease of regeneration of the solvent requires making a choice between energy-intensive processes for the regeneration of the solvent or working with small amounts of CO_2 repeatedly for separation with high purity. Also different pressure and temperature conditions require different solvents and NO_x and SO_x

components of the flue gas may degrade the solvent. This method can be improved by identifying better solvents or redesigning the regeneration procedures [3].

Adsorption occurs between a solid adsorbent and the gaseous mixture. The CO_2 molecules are physi-sorbed by the surface groups of the adsorbent with the effect of temperature, partial pressure of CO_2, interaction energy between sorbent and CO_2, pore size and available surface area of the sorbent. Adsorption-based separation is comparatively easy to perform but has the disadvantages of slow rate, low selectivity and low working capacity. By development of better adsorbents with higher working capacity, higher selectivity, flexible working conditions and capable packing structures, adsorption-based separation of CO_2 from flue gas can be a feasible method for CO_2 capture [2].

In cryogenic distillation, the mixture containing only CO_2 and N_2 is distilled under high pressure and extremely low temperature to a point where CO_2 is liquefied but N_2 remains in its gaseous phase. This method offers an advantage of easy transportation of liquefied CO_2 with a pipeline or tanker, but its limitations such as requiring the CO_2/N_2 mixture to be purified from other components of the flue gas before operation and high-energy requirement need to be optimized before it can be used cost-effectively [2].

Membrane-based CO_2/N_2 separation has been a powerful alternative to the traditional separation methods such as distillation, absorption, and adsorption due to its low cost, energy efficiency and smaller ecological footprint [4]. The advantage of membrane-based separation is that when only a pressure gradient is applied to a suitable membrane which can interact with CO_2 and remain stable under the experimental conditions, the membrane can separate the targeted molecule which is able to dissolve or absorb into the membrane and diffuse into the pores [2]. Membranes are easy able to install and do not require expensive chemicals or high energy consumption and therefore regarded as a promising method for CO_2 capture.

In membrane-based separation, CO_2 in the flue gas stream entering into the separation tank diffuses into the membrane while other components leave the tank untreated. Due to the pressure difference between feed and permeate sides of the membrane, CO_2 in flue gas

is drawn into the membrane. At the end, retentate stream contains the untreated components while permeate stream contains the CO_2 separated from flue gas [5]. In Figure 1.1 this process is shown.

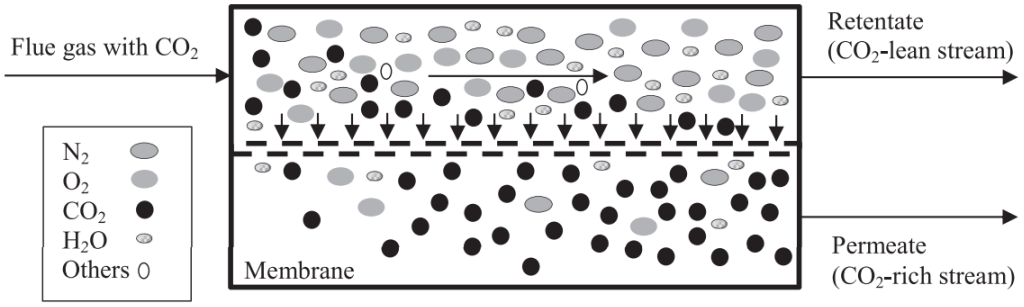

Figure 1.1 Schematic of membrane-based separation for CO_2 capture from flue gas.[5]

Various types of membranes are available such as inorganic, metallic, polymeric or solid-liquid. While polymeric membranes have been widely used for membrane-based gas separation, there is a trade-off between the gas permeability and selectivity of polymeric membranes as shown by Robeson [6, 7]. One way to enhance the performance of polymeric membranes is the fabrication of mixed matrix membranes (MMMs) in which nanoporous materials such as zeolites,[8, 9] carbon nanotubes, [9, 10] zeolite imidazolate frameworks (ZIFs),[11, 12] carbon molecular sieves [9, 13] or metal organic frameworks (MOFs) [14, 15] are incorporated into polymers. Among these fillers, MOFs and ZIFs represent a relatively new group of crystalline nanoporous materials. MOFs are composed of metal ions linked by organic bridging ligands whereas ZIFs are a subfamily of MOFs composed of tetrahedral networks consisting of transition metal ions and imidazolate linkers [16, 17]. MOFs and ZIFs have received significant attention in the last decade for gas storage and gas separation due to their large surface areas, high pore volumes, well-defined pores and tunable chemistries [18, 19]. Ma et al. [20] recently synthesized a series of MOFs named as porous coordination networks (PCNs) that offer large surface area, high

porosity, tunable pore size and good chemical and thermal stability. These properties make PCNs promising candidates for gas storage and separation. Although many MOFs and ZIFs were used as filler particles in polymers, no PCN has been used as fillers in MMM applications up to date. Considering the large numbers of available PCNs and polymers in the literature, it is challenging to experimentally identify the best PCN/polymer pairs for high-efficiency CO_2/N_2 separation. In this thesis, we combined molecular simulations with theoretical permeation models to predict the CO_2/N_2 separation performance of 200 different PCN-based MMMs for the first time in the literature.

Simulation is an important aspect of research for the investigation of gas separation performance of membranes as it provides a quick tool which makes it possible to reproduce the observations of an experimental work without repeating the energy-intensive experimental procedure or gives a clue about the gas separation performance of not-yet synthesized membranes. It can also give more insight about a system such as specific adsorption sites and interaction mechanisms, gas uptake and heats of adsorption for various adsorbents and examinations about dynamic properties of gas solid systems. Computational methods also make it possible to determine some structural properties such as accessible surface area and free volume of micropores which are difficult to examine experimentally [21]. Therefore, combination of computational investigation of a system with experimental work can provide information about that system with high accuracy.

To accomplish the aim of this thesis, first a polymer set was created which consisted of the polymers which were already commercially used or available to overcome the Robeson's upper bound with a little improvement when combined with PCNs. As an important amount of data about gas permeability of polymers was available in the literature, CO_2 and N_2 permeability of polymers were collected from the literature. Before implementing the computational methodology to PCNs, the computational methodology is validated with comparing the results of the available experimental work on MOF and ZIF based MMMs with simulation results of this work. After observing a good agreement between simulation results and experimental results, CO_2 and N_2 permeability of PCNs

were calculated with computational methods. These were combined in theoretical models which determined gas separation performance of PCN-based MMMs. Several PCNs which were able to carry polymers over the Robeson's upper bound were identified as promising PCNs and promises of these PCNs were further investigated with evaluating the effect of PCN loading and PCN flexibility on the gas separation performance of PCN-based MMMs.

Chapter 2 provides a literature review that discusses experimental and computational studies on PCN, MOF and ZIF-based MMMs. In Chapter 3, details of the computational methodology which was used to calculate the gas permeability and selectivity of PCNs and PCN-based MMMs are summarized. Information about the use of Grand Canonical Monte Carlo [22] and Equilibrium Molecular Dynamics [22] are given in that chapter. Determination of structural properties of PCNs with computational methods is also explained in Chapter 3. Last of all, theoretical models which are applied to calculate gas permeability of PCN-based MMMs are explained. In Chapter 4, validation of the computational methodology is provided with comparing the simulation results with the results of the available experimental work on MOF and ZIF-based MMMs in the literature as PCN-based MMMs were not experimentally investigated yet. After validating our computational method, results for the gas permeability of PCNs and PCN-based MMMs are given in Chapter 4. Performances of the new PCN-based MMMs were evaluated by considering permeability and selectivity of the MMMs. This chapter is concluded with the investigation of the effect of PCN loading and PCN flexibility on the performance of PCN-based MMMs. With that the conditions under which PCN flexibility was effective for the performance of the MMM were identified. In Chapter 5, concluding remarks and future work are provided.

Chapter 2

LITERATURE REVIEW

In membrane-based separation, both solubility and diffusivity of the gas molecules contribute to the selective transport of gas molecules. Gas molecules first dissolve into the membrane at the upstream (high) pressure, diffuse across the membrane and desorb at the downstream (low) pressure as shown in Figure 2.1 [23]. If the conditions for strong adsorption and fast diffusion of gas molecules could be achieved at the same time, desired separation efficiency could be obtained [24].

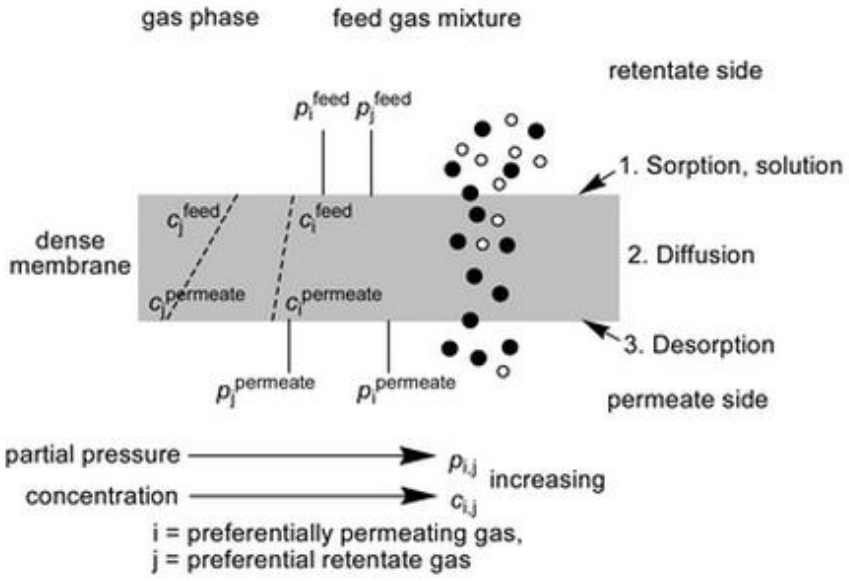

Figure 2.1 Membrane-based separation via solution-diffusion mechanism[25]

These two processes, solution of the gas molecules and diffusion through the membrane, determine the permeability of a gas through the membrane. The ratio of the gas permeability of a membrane for two different gases is identified as the ideal selectivity of that membrane. It also equals to the product of the ratio of the diffusivity and the ratio of the solubility of the two gases. Polymeric membranes are mostly preferred in membrane-based gas separation due to the ease of fabrication of polymers, lower cost, higher mechanical stability and easier scalability [25, 26]. Permeability and selectivity are the two most important properties of polymeric membranes. Polymers with high permeability decrease the unit area required to treat a specific amount of gas while polymers with high selectivity result in separation with high purity. However, there is a trade-off between permeability and selectivity such as a polymer with high permeability has low selectivity and vice versa [6, 7]. Increasing the selectivity requires either increasing the solubility or diffusivity of the gas molecule, but polymeric membranes have defined properties which cannot be easily adjusted without chemical modifications [27].

For CO_2/N_2 separation, membrane-based gas separation is evaluated as a promising method to be preferred over conventional methods in the future when especially the concerns related to permeability/selectivity trade-off, membrane preparation and stability are relieved [2]. As a means of enhancing the performance of polymeric membranes, preparation of MMMs is being considered which enables combining the advantages of polymeric membranes with the advantages of the fillers. These filler materials include carbon nanotubes, zeolites, metal organic frameworks and carbon molecular sieves as mentioned in Chapter 1. Due to the easier adjustability of their surfaces with various functional groups, MOFs, ZIFs and their MMMs provide many advantages for membrane-based gas separation. This chapter is a literature review about the performance of MOFs, ZIFs, PCNs and their MMMs used for CO_2/N_2 separation.

2.1 Mixed Matrix Membrane (MMM)

Robeson has identified an upper bound for polymeric membranes by collecting the permeability and selectivity data of a large set of polymers for industrially relevant gas mixtures [6, 7]. This upper bound is a graphical demonstration of the trade-off between permeability and selectivity of polymers. As it is shown in Figure 2.2 among the upper bounds identified for several gas mixtures, the highest upper bound is for CO_2/N_2 separation.

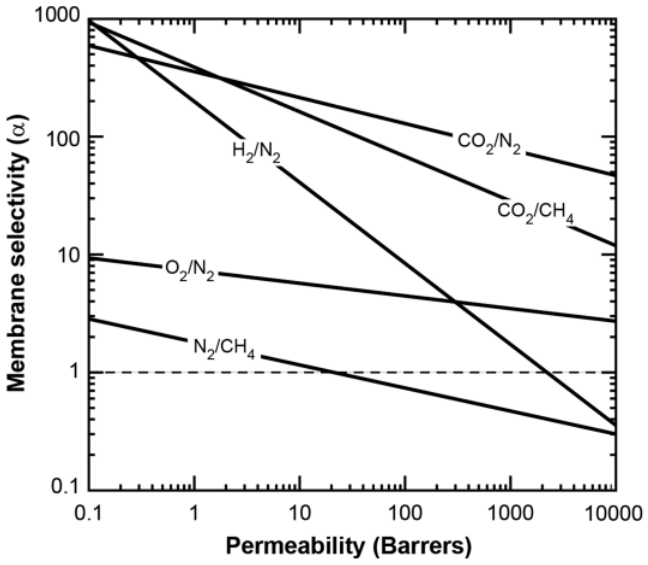

Figure 2.2 Robeson's upper bounds identified for several gas mixtures [28]

It is desired to obtain membranes which are at the right-hand corner of this figure, having high permeability and high selectivity at the same time. Different methods have been developed to enhance the performance of polymeric membranes such as blending two polymers, modification of membrane surfaces, and chemical cross-linking of polymers [29].

Despite these efforts, performance of the polymeric membranes could not overcome the trade-off of permeability vs selectivity as much as it is intended. Design of new MMMs were another choice to boost the performance of polymeric membranes for gas separation. MMMs are composite membranes in which an inorganic phase is dispersed into the polymer which is the continuous phase. With combining these two phases, the advantages of polymer phase such as easy processibility, low cost and mechanical stability are enhanced with the advantages that the inorganic phase provides such as high mechanical and thermal stability, high gas permeability and selectivity. Most of all, MMMs consist of zeolite particles immersed in polymers. In Figure 2.3, selectivity and permeability of polymeric membranes, inorganic membranes and MMMs are shown together with Robeson's present and previous upper bounds [6, 7]. Present upper bound is the updated version of the previous upper bound with the addition of the new data about polymers [7].

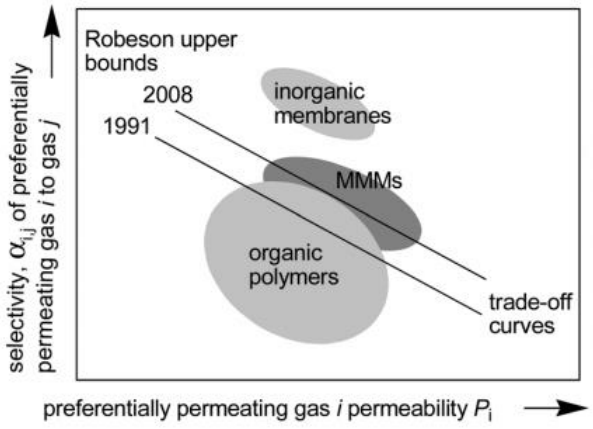

Figure 2.3 Gas separation performance of polymer membranes, inorganic membranes, and MMMs together with Robeson's upper bound. [25]

Although zeolites are able to improve the permeability and selectivity of the MMMs they are used in, there are some drawbacks of utilizing zeolites in MMMs. For example,

manufacturing defect-free zeolites is not an easy task, pores of zeolites could be blocked by polymers, number of possible zeolites structures is limited and there is also a compatibility problem between zeolites and polymers which leads to defects in the MMMs and therefore poor gas-separation performance [25, 30]. Compatibility of the inorganic phase with the organic phase (polymer) is very important for the selective separation of gases. Among inorganic filler choices, MOFs have represented a better structural compatibility than zeolites with the polymer phase [31]. Also, MOFs are easier to synthesize, variations of MOFs are unlimited and their adhesion to the polymer phase could be more easily improved. By combining MOFs with the polymers, the problems associated with MOF membranes such as fragility and difficult manufacturing can be eliminated. The preparation method of MOF-based MMMs is shown in Figure 2.3.

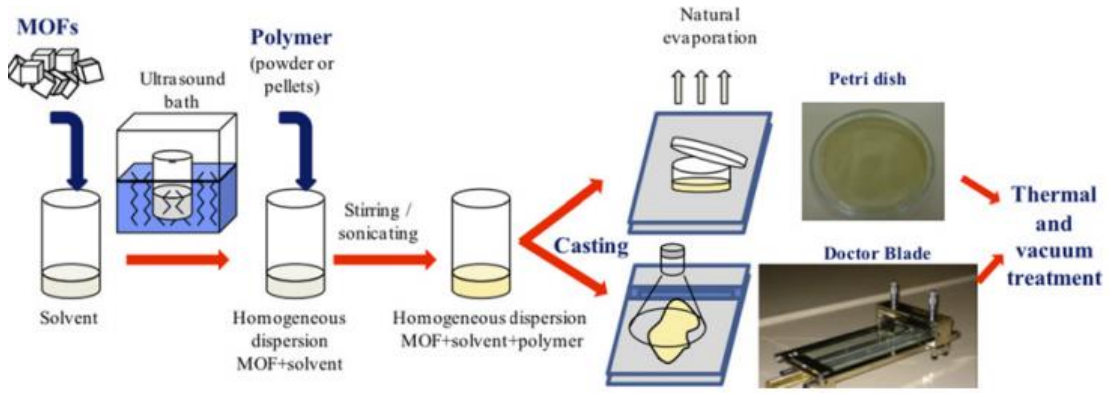

Figure 2.4 Preparation of MOF-based MMMs [32]

In MOF-based MMM preparation, MOF is first dispersed in a solvent in the ultrasonic bath. Polymer phase is added in a ratio of 90/10 wt.% solvent/filler-polymer mixture. This mixture is stirred overnight with sonication. When a homogeneous mixture of MOF and polymer in the solvent is obtained, the membranes are ready to be casted on a flat surface, like a petri dish or a doctor blade. These membranes are left overnight for the evaporation

of the solvent at room temperature. Dried films are kept in vacuum oven for 24 hour at a temperature, which is set with respect to the glass transition temperature of the polymer, to eliminate the remaining amount of solvent in the membrane [32].

MOF-based MMM studies are implemented on theoretical basis using various permeation models including Maxwell, Bruggeman, Lewis-Nielson, Pal, Modified-Maxwell, Felske, and Modified Felske. With these permeation models, pure gas permeability of the MMM can be predicted. These models are mostly originated from the thermal and /or electrical conductivity models. Among these various models Maxwell, Bruggeman, Lewis-Nielson and Pal models assume ideal morphology between the polymer phase and the filler. Ideal morphology means that the polymer phase and the inorganic phase are completely compatible to form a homogeneous membrane. These models are valid for low to moderate volume fraction of fillers. Others take into account the effect of the rigidified layer in the polymer-filler interface [33].

Separation of CO_2 from flue gas via membrane-based separation has some difficulties which has to be overcome. These include the low feed gas pressure, low concentration of CO_2 and high gas flow rate. Development of MMMs opens a route for the design of better membranes for CO_2 capture from flue gas. Dong et al. [34] lists various MMMs including Matrimid/MOF-5 MMM which has shown promising performances for this application. With the continuous development on this area, MMMs are believed to be used in various gas separations in the future.

2.2 MOFs and ZIFs for CO_2/N_2 separation

Metal organic frameworks (MOFs) and zeolitic imidazolate frameworks (ZIFs) have the advantage of tailorability of their properties. Their pore sizes, functional groups, and surface areas can be adjusted to obtain higher CO_2/N_2 selectivity. With the motivation of having materials with even better properties, many MOFs and ZIFs have been studied

for CO_2/N_2 separation. For example, as adsorbents MOF-177 overcome the previous highest CO_2 uptake capacity at room temperature with exceeding the uptake capacities of known MOFs such as IRMOF-1, IRMOF-3, IRMOF-6, IRMOF-11, CuBTC (HKUST-1), MOF-74, MOF-505 [35]. CuBTC [35], MOF-177 [35], MOF-5 [35], IRMOF-3 [35], and ZIF-8 [36] have overcome the CO_2 adsorption performances of various zeolites [37]. Mg-MOF-74 offered high CO_2 adsorption at low pressures due to the strong interaction of its unsaturated metal sites with CO_2 molecules [38]. As membranes, Liu et al. [39] reported that, with ZIF-69 a relatively higher CO_2/N_2 separation factor was obtained. Guerrero et al. [40] observed that CO_2 permeance in HKUST-1 was higher than the permeance of N_2 at increased temperature.

Besides the experimental works, computational work on MOF based CO_2/N_2 separation has been also making valuable contributions to this area. In 2007, Yang et al. [41] performed a computational study to examine the performance of HKUST-1 for flue gas separation with simulating one, two, and three-component mixture for $CO_2/N_2/O_2$ and showed that CuBTC is a promising MOF for flue gas separation. It is also observed that composition, pressure and temperature have significant effects on the gas adsorption. Zhang et al. [42] worked on the CO_2 separation capability of Cu-TDPAT using computational methods and determined that Cu-TDPAT has a high CO_2/N_2 selectivity.

2.3 MOF and ZIF-based MMMs for CO_2/N_2 separation

The permeability and selectivity of MOF and ZIF-based MMMs for CO_2/N_2 separation have been investigated by several experimental studies. Bae and Long [43] investigated the CO_2/N_2 separation performance of three different MMMs consisting of polymers polydimethylsiloxane (PDMS), cross-linked polyethylene oxide (XLPEO), polyimide (PI), 6FDA-TMPDA (6FDA:2,2′ bis(3,4′-dicarboxyphenyl)hexafluoropropane dianhydride and TMPDA: 2,4,6-trimethyl-1,3-phenylenediamine) and Mg-MOF-74 as fillers. They found

that pure CO_2 and N_2 permeability of the MMMs based on PDMS and XLPEO decreased while CO_2/N_2 selectivity was improved slightly compared to pure polymer membranes. The decrease in permeability of these two MMMs was explained by plugging of the pores of Mg-MOF-74 by the rubbery polymers, PDMS and XLPEO. The MMM based on glassy polymer, PI, showed higher CO_2 permeability and CO_2/N_2 selectivity compared to unfilled polymer. Japip et al. [44] incorporated nano-sized ZIF-71 particles into 6FDA-Durene (Durene diamine: 2,3,5,6-tetramethyl-1,4-phenylenediamine) and observed enhanced CO_2 and N_2 permeabilities. However, the ideal selectivity for CO_2/N_2 decreased from 14.7 to 11.5 with 30 wt% ZIF-71 in 6FDA-Durene polyimide. Nafisi and Hägg [45] examined the CO_2/N_2 separation performance of ZIF-8 incorporated into 6FDA-Durene diamine MMM using single gases (CO_2 and N_2) and binary gas mixtures (10% CO_2 and 90% N_2). They found that CO_2 and N_2 permeabilities of the MMM increased both in single gas and binary gas measurements as the weight fraction of ZIF-8 in the polymer increases. Lin et al. [46] designed a MMM which consists of Cd-6F nanoparticles in 6FDA-ODA (ODA:oxydianiline) polyimide. They observed a significant increase in pure CO_2 permeability and selectivity of the Cd-6F filled 6FDA-ODA MMM compared to pure 6FDA-ODA. Another MOF-based MMM tested for CO_2/N_2 separation was CuBTC/Ultem.[47] The CO_2 and N_2 permeability of MMM increased whereas the CO_2/N_2 selectivity remained almost same compared to pure polymer at 35 wt% of CuBTC. CuTPA/PVAc (polyvinyl acetate) MMMs synthesized by Adams et al. [30] with 15 wt% CuTPA showed improved CO_2 and N_2 permeability and improved CO_2/N_2 selectivity with respect to the performance of the pure polymer membrane. Basu et al. [48] examined two MOF and ZIF-based MMMs prepared with ZIF-8 and CuBTC immersed in Matrimid. Both of the membranes have shown increased permeability and selectivity compared to pure polymer.

The number of computational studies on MOF and ZIF-based MMMs for CO_2/N_2 separation is very limited compared to experimental studies. Erucar et al. [49] investigated the effects of electrostatic interactions between adsorbate molecules and MOF structure on CO_2 and N_2 permeability of MOF-based MMMs using molecular simulations. It was concluded that considering electrostatic interactions has a significant effect on the result of CO_2 and N_2 permeability of pure MOF membranes but less importance on the permeability of MOF-based MMMs. Yilmaz and Keskin [50] estimated separation performances of new MMMs composed of various MOFs and ZIFs as fillers. Several MOFs and ZIFs were identified as promising fillers to carry polymers above the upper bound for CO_2/N_2 separation by enhancing both CO_2 permeability and CO_2/N_2 selectivity.

2.4 Porous Coordination Networks (PCNs)

Starting with the aim of increasing the gas affinity of metal centers in MOFs for hydrogen uptake, Ma et al. [51] recently synthesized a series of MOFs named as porous coordination networks (PCNs) that offer large surface area, high porosity, tunable pore size and good chemical and thermal stability. These properties make PCNs promising candidates for gas storage and separation. For example Lu et al. [52] determined CO_2 and N_2 adsorption in PCN-80 which offers high open-metal site density when it is activated. PCN-80 presented high CO_2 uptake capacity and little N_2 uptake capacity which led to a high adsorption selectivity for CO_2/N_2, 18.7 at 273 K and 11.8 at 296 K. Jiang et al. [53] introduced various functional groups into highly stable isoreticular Zr-based PCNs and examined CO_2/N_2 adsorption selectivity of PCNs -56, -57, -58 and -59. Zhuang et al. [54] measured CO_2 and N_2 adsorption in PCN-26 and reported high CO_2/N_2 selectivity of 49, one of the highest adsorption selectivities compared to widely studied MOFs. PCN-305, -306, -307, and -308 [55] were also studied for adsorption-based separation of CO_2/N_2. Liu

et al. [56] reported that PCN-72 is a promising material for CO_2 capture from flue gas as it is thermally and mechanically stable while it is also highly selective for CO_2 over N_2.

In addition to these experimental studies, molecular simulations are also used to examine adsorption and separation properties of PCNs. Zhuang et al. [54] performed molecular simulations to investigate CO_2 adsorption sites in PCN-26. Babarao et al. [57] investigated the effects of functional groups on CO_2 capture and found that due to the strong electrostatic interactions between the hydroxyl groups of the framework and CO_2 molecules, PCN-59 showed a considerably higher selectivity than the other frameworks (PCN-56, 57, 58) for two-component CO_2/N_2 (15:85) mixture. They also examined the effect of impurities in flue gas mixture on CO_2 adsorption with considering two, three, and four component gas mixtures (such as CO_2/N_2,$CO_2/N_2/O_2$, $CO_2/N_2/H_2O$, $CO_2/N_2/H_2O/SO_2$) molecular simulations and found that only H_2O affected the CO_2 selectivity in all frameworks. Ozturk and Keskin [58] used atomically detailed simulations to investigate both adsorption-based and membrane-based gas separation performances of various PCNs for industrially important gas separations including CO_2/N_2. They computed adsorption-based selectivity, diffusion-based selectivity, membrane-based selectivity and gas permeability of PCNs and showed that PCNs can outperform widely studied zeolites and MOFs. PCN-26 was identified as a good candidate for membrane-based CO_2/N_2 separation by exceeding the Robeson's upper bound. In a following work, Ozturk and Keskin [59] studied adsorption-based and membrane-based gas separation performance of 20 different PCNs and suggested approximate models that can give an initial estimate about the adsorbent and membrane selectivity of a PCN depending on its structural properties such as pore volume, surface area.

As the literature survey summarized so far shows PCNs are promising materials in gas separation applications. Although many MOFs and ZIFs were used as filler particles in polymers, no PCN has been used as fillers in MMM applications up to date. In this work,

CO_2/N_2 separation performance of 200 PCN-based MMMs is rapidly screened with computational methods and these calculations identified several PCN-based MMMs that can overcome Robeson's upper bound for CO_2/N_2 separation.

Chapter 3

COMPUTATIONAL DETAILS

In this chapter, utilization of Grand Canonical Monte Carlo (GCMC) simulations and Equilibrium Molecular Dynamics (EMD) simulations for the determination of gas permeability of PCNs is summarized and methods to computationally determine the structural properties of PCNs are explained. Following that, theoretical models used to calculate gas permeability of PCN-based MMMs are discussed.

3.1 Selection of PCNs and polymers

We studied 20 different types of PCNs as filler particles in MMMs. These are PCN-6, -6', -9-Fe, -9-Co, -9-Mn, -10, -11, -13, -14, -16, -16', -18, -19, -20, -26, -39, -46, -80, -131' and -224-Ni. These PCNs were chosen since they were identified as promising adsorbent and membrane materials for several gas separations in recent studies [58, 59]. In addition to these materials, CuBTC,[47, 60, 61, 62] CuTPA,[30] IRMOF-1,[63, 64] ZIF-8,[12, 45, 65, 66, 67] ZIF-71,[44] ZIF-90,[11] Mg-MOF-74,[43] and Cd-6F[46] were also studied as filler particles because there is a large amount of experimental data available in the literature for CO_2 and N_2 permeability of MMMs that include these MOFs as fillers.

Polymers studied in this work were Matrimid,[64] Ultem,[66], 6FDA-DAM (2,2-bis(3,4-carboxyphenyl) hexafluoropropane dianhydride-diaminomesitylene),[68] polyimide (TADATO/DSDA(1/1)–DDBT),[69] poli(bis(2-(2-methoxyethoxy)ethoxy)phosphazene) (MEEP),[70] polymers of intrinsic microporosity (PIM-1 and PIM-7),[71] modified PDMS (poli(dimethylsiloxane)),[72] PVAc,[30] PI,[43] 6FDA-ODA,[46] 6FDA-Durene,[44, 45]

poli(trimethylgermylpropyne) (PTMGP),[73] and poli(trimethylsilylpropyne) (PTMSP) [73]. These polymers are located at different regions of the selectivity vs. permeability graph with respect to Robeson's upper bound for CO_2/N_2 separation [7]. For example, Matrimid [64] has a moderate CO_2 permeability (9 Barrer) but high CO_2/N_2 selectivity (36) while PTMGP [73] has a high CO_2 permeability (14000 Barrer) but moderate selectivity (14). Polymers such as Matrimid, Ultem, 6FDA-DAM, PDMS were considered in this work since they are the most widely used polymers in the experimental MMM studies for CO_2/N_2 separations. Polymers such as PIM-1, PIM-7, PTMSP were specifically studied since they are close to the upper bound and they may exceed the upper bound if appropriate filler particles having high CO_2 selectivity and/or high CO_2 permeability are incorporated into them.

3.2 Calculation of gas permeability of PCNs using molecular simulations

In order to predict gas permeability of new PCN-based MMMs, which have not been fabricated to date, gas permeability data of pure PCNs and polymers are required. Gas permeability of PCNs was calculated using molecular simulations while gas permeability of polymers was obtained from the literature. To start with the simulation of PCNs, the crystal structures of solvent-free, rigid PCNs were obtained from the experimentally reported files in the Cambridge Structural Database (www.ccdc.cam.ac.uk) using their six-letter reference codes. For every PCN, this crystallographic data including the crystal type (cubic, hexagonal, orthorhombic, or tetragonal), x,y,z atomic coordinates, a,b,c unit cell lengths and α, β, γ unit cell angles were prepared in an appropriate format to be used in simulations. Molecular simulations for PCNs were performed at 298 K and at a feed (permeate) pressure of 2 bar (vacuum) to be consistent with the permeance conditions of polymeric membranes.

3.2.1 Grand Canonical Monte Carlo (GCMC)

Single-component adsorption of gases was computed using Grand Canonical Monte Carlo (GCMC) simulations. Grand Canonical Monte Carlo simulation is a widely used technique to determine gas-solid adsorption in which chemical potential (μ), volume (V) and temperature (T) are kept constant while number of adsorbed molecules (N) is allowed to fluctuate [22]. It requires a force field which provides the parameters required for the calculation of energetic interactions. These energetic interactions include dispersion forces and electrostatic interactions. Electrostatic interactions were taken into account using the Coulomb potential and LJ 12-6 potentials were used to model repulsion and dispersion forces [74] as shown in Equation 3.1.

$$U(r_{ij}) = 4\varepsilon_{ij}\left[\left(\frac{\sigma_{ij}}{r_{ij}}\right)^{12} - \left(\frac{\sigma_{ij}}{r_{ij}}\right)^{6}\right] + \frac{1}{4\pi\varepsilon_0}\frac{q_i q_j}{r_{ij}} \qquad (3.1)$$

Here, U is the potential energy between two atoms i and j at a distance r, q_i is the partial charge on atom i, ε_{ij} is LJ potential well depth and σ_{ij} is LJ potential diameter, and ε_0 is the dielectric constant. Lorentz-Berthelot mixing rules were used to calculate cross interaction parameters between dissimilar atoms, as shown in Equation 3.2.

$$\sigma_{ij} = \frac{\sigma_{ii} + \sigma_{jj}}{2} \qquad \varepsilon_{ij} = \sqrt{\varepsilon_{ii}\varepsilon_{jj}} \qquad (3.2)$$

To describe the interactions between PCN atoms and gas molecules, there are several force fields such as universal force field (UFF) [75], Dreiding force field [76] and optimized potential for liquid simulations all-atom (OPLS-AA) [77] force field. In this

thesis, Dreiding force field [76] was used to define LJ potential parameters of PCNs. For metal atoms, potential parameters were taken from UFF [75] since they were not available in Dreiding force field. Ozturk and Keskin [58, 59] showed that molecular simulations based on Dreiding give very good agreement for CH_4, CO_2, H_2 and N_2 adsorption in PCN-26, H_2 adsorption in PCN-6, -6', -10, -11, -14, -16, -20, -80 and -46, CH_4 adsorption in PCN-11, -14, -16, -46 and -80, and CO_2 adsorption in PCN-46 and -80. The energetic potential parameter (ε) of carbon atom of PCN-26 was slightly modified to provide a better agreement between the experimentally measured adsorption data and simulation results following Ozturk and Keskin [58].

In order to simulate the adsorbate molecules, the CO_2 molecule was modeled as a rigid, three-site molecule with LJ 12-6 potential, and partial point charges were located at the center of each site.[78] The N_2 molecule was modeled as a three-site molecule with two sites located at the N atoms and the third site located at the center of mass with partial point charges.[79] These values are also shown in Table 3.1.

Table 3.1 Parameters used in the modelling of adsorbate molecules

Gas	Atom	σ (Å)	ε/k_b (K)	q(e)
CO_2	C	2.80	27.00	0.70
	O	3.05	79.00	-0.35
N_2	N	3.31	36.40	-0.40
	COM	0.00	0.00	0.80

In order to calculate the electrostatic interactions partial point charges for PCN atoms are required. There are several atomic partial charge calculation methods such as extended charge equilibration method (EQeq) [80], connectivity-based atom contribution method (CBAC) [81, 82], repeating electrostatic potential extracted atomic charges (REPEAT) method [83], density-derived electrostatic and chemical charges (DDEC) method [84] and

electrostatic potential energy surface method [85]. In this thesis, partial point charges were assigned to PCNs using extended charge equilibration (EQeq) method [80] for computing the electrostatic interactions between CO_2 molecules-PCNs and N_2 molecules-PCNs. This method, which utilizes ionization potentials and electron affinities of the transition metal atoms at their oxidation states, provides a quick and accurate assignment of atomic charges to PCNs as shown in previous works of Ozturk and Keskin [58, 59]. The cut-off radius for intermolecular (electrostatic) interactions was set to 13 (25) Å. Simulation box was consisted of 2×2×2 unit cells and periodic boundary conditions were applied to simulate the bulk phase. 1.5×10^7 equilibration and 1.5×10^7 production steps were used. Four types of different moves were employed during the simulations which are insertion (creates a new molecule in a random position with random orientation), deletion (randomly deletes an existing molecule), rotation (rotates an existing molecule that is randomly selected, not required for spherical molecules) and translation (randomly selects and translates an existing molecule). Amount of adsorbed molecules under specified conditions obtained from the GCMC simulations were further used in equilibrium molecular dynamics simulations.

3.2.2 Equilibrium Molecular Dynamics (EMD)

An Equilibrium Molecular Dynamics (EMD) simulation solves the equation of motion for N particles in three dimensions. It utilizes Einstein's relation to calculate the diffusivity of the adsorbed molecules with taking the slope of the mean square displacement with respect to time [22]. In this work, EMD simulations in NVT ensemble (NVT = constant number of molecules, constant volume and temperature) were performed to calculate the corrected diffusivity (D_0) of gases.

The corrected diffusivity represents the collective motion of the adsorbed molecules and is calculated based on the number of molecules (N), time (t), the three dimensional position vector of molecule l of species i at time t, $r_{il}(t)$ [22].

$$D_{0,i} = \lim_{t\to\infty} \frac{1}{6Nt} \left\langle \left(\sum_{l=1}^{N_i} \left[r_{il}(t) - r_{il}(0) \right] \right)^2 \right\rangle \tag{3.3}$$

Temperature was kept constant by applying Nosé-Hoover thermostat algorithm [22]. At least 20 trajectories were collected from EMD simulations and average corrected diffusivity was reported. The transport diffusivity (D_t) was obtained by multiplying the corrected diffusivity (D_0) with thermodynamic correction factor ($\partial \ln f / \partial \ln c$),[86] the partial derivative relating the adsorbed gas amount, c and bulk phase fugacity, f.

$$D_t(c) = D_0(c) \cdot \frac{\partial \ln f}{\partial \ln c} \tag{3.4}$$

3.2.3 Calculation of gas permeability of PCNs

The shell model was applied to calculate the steady state fluxes of each gas molecule through a PCN based on Fick's Law:[86]

$$J = -D_t(c) \cdot \nabla c \tag{3.5}$$

Here, ∇c is the concentration gradient of the adsorbed species based on the difference between the feed and permeate side pressures of the membrane. Gas flux (J) in PCNs was then converted to gas permeability in filler (PCN) (P_f) using following formula,

$$P_f = \frac{J}{\Delta P / L} \tag{3.6}$$

where ΔP is the pressure drop and L is the membrane thickness. All permeability data are given in the units of Barrer [87] which corresponds to,

$$1 \text{ Barrer} = \frac{10^{-10} cm^3 (STP).cm}{s.cm^2.cmHg} \tag{3.7}$$

Ideal selectivity (S) of PCNs was calculated as the ratio of gas permeability of two components:

$$S_{i/j} = \frac{P_{f_i}}{P_{f_j}} \tag{3.8}$$

3.3 Calculation of structural properties of PCNs

To better evaluate the performance of PCNs, structural properties need to be determined. In this work, accessible surface area, pore volume and pore diameter of the PCNs were taken into consideration.

Accessible surface area was calculated with a Monte Carlo integration method proposed by Duren et al. [88]. In this method, accessible surface area is determined by rolling a spherical probe particle over the framework surface of a MOF and calculating the fraction of the points where probe particle does not overlap with the framework atom. Overlapping is determined via considering the size (σ) of the framework atoms and the probe molecule.

$$S_{acc,i} = \frac{M_{i,no-overlap}}{M_{i,total}} . \pi . \sigma_i^2 \tag{3.9}$$

Here, $M_{i,no-overlap}$ is the number of random points that do not overlap with a framework atom, $M_{i,total}$ is the number of total random points, and σ_i is the sum of the size of the framework atom and the probe particle. It is worth to note that, as the surface area of PCNs is experimentally determined mostly through Brauner-Emmett-Teller (BET) analysis with N_2 adsorption at 77 K [89], the size of the probe particle should be in accordance with the size of the N_2 molecule to be consistent with the experimental measurement results,[90] therefore a probe with the size of a N_2 molecule (3.68 Å) was used in these measurements. Total accessible surface area was determined with summing all individual surface areas determined for an atom as shown in Equation 3.10. These measurements were done under 298 K.

$$S_{acc} = \sum_{i=1}^{N} S_{acc,i} \tag{3.10}$$

Pore volume, largest cavity diameter (LCD) and limiting pore diameter (LPD) are other important parameters considered in the examination of the gas separation performance of PCNs. In this work, these properties were calculated with the Poreblazer method proposed by Sarkisov et al. [91]. Pore volume was calculated with the method of Myers and Monson [92] which is based on the absolute adsorption second virial coefficient. Then, pore volume was calculated with the following equation,

$$V_{pore} = \frac{1}{m} \int e^{-E(r)/k_B T} dr \tag{3.11}$$

Here E is the fluid-adsorbent interaction energy of a single helium atom at position r and m is the mass of the adsorbent. With applying a Monte Carlo technique, integration over the entire adsorbent was done. In the pores, the exponential can be calculated but inside the nonporous regions of the adsorbent E goes to infinity.

In pore volume calculations, a Helium probe with a kinetic diameter of 2.58 Å and energy parameter of 10.22 K was used. These calculations were done under 298 K to be consistent with the experimental determination of helium-based pore volume.

Pore size was calculated with two Monte Carlo procedures which start with dividing the pore range of interest into small bins. First Monte Carlo procedure locates a point in the adsorbent which should not overlap with other adsorbent atoms. Second Monte Carlo procedure determines the largest sphere containing the point with navigating the pore space of the adsorbent with a probe. After determining the size of the largest sphere, the value of the bin corresponding to that radius and smaller radii were increased by one.

LPD and LCD are the maximum size of the molecule that can go through the major pore channel and maximum size of a molecule that can be inserted into the structure, respectively. LPD is not necessarily equivalent to LCD as frameworks might have multiple pore channels with limited connectivity and LCD might not be in the major pore. [93]

3.4 Calculation of gas permeability of PCN-based MMMs

In a recent work, Erucar and Keskin [94] tested several theoretical permeation models, namely Maxwell, modified Maxwell, Bruggeman, Lewis-Nielson, Pal, Felske and modified Felske by comparing predictions of these models with a large set of experimental data for gas permeability of MOF-based MMMs. It was concluded that Maxwell model is the best predicting permeation model among the models based on the ideal morphology concept. In this study, Maxwell and modified Maxwell models were used to predict the gas permeability of PCN-based MMMs. Maxwell model [95] predicts the MMM's gas permeability (P) based on the polymer's permeability (P_p), filler particles' permeability (P_f) and volume fraction of the filler particles within the polymer matrix (ϕ).

$$P = P_p\left[\frac{2(1-\phi)+(1+2\phi)\lambda_{fp}}{(2+\phi)+(1-\phi)\lambda_{fp}}\right] \tag{3.12}$$

$$\lambda_{fp} = \frac{P_f}{P_p} \tag{3.13}$$

Maxwell model is known to make accurate predictions at low to moderate volume fraction ($0<\phi<0.3$) of filler particles [33]. It assumes ideal morphology, which means there is a perfect compatibility between the filler particles and polymer, and it does not consider the particle size distribution, particle shape and aggregation of particles.

Modified Maxwell model [96] includes the effects of rigidification of the polymer-filler interface and considers an MMM as an idealized two-phase system including polymer matrix phase and combined phase of dispersed particles (filler particles)/interface (pseudo-insert phase).

$$P_{eff} = P_I\left[\frac{2(1-\phi_s)+(1+2\phi_s)(P_f/P_I)}{(2+\phi_s)+(1-\phi_s)(P_f/P_I)}\right] \tag{3.14}$$

$$P_I = \frac{P_p}{\beta^*} \tag{3.15}$$

$$\phi_s = \frac{\phi}{\phi+\phi_I} \tag{3.16}$$

$$P = P_p\left[\frac{2(1-\phi)+(1+2\phi)(P_{eff}/P_p)}{(2+\phi)+(1-\phi)(P_{eff}/P_p)}\right] \tag{3.17}$$

Here, P_{eff} is the effective permeability of the pseudo-insert phase, P_I is the permeability of the interphase, β^* is the matrix rigidification factor, ϕ_s is the volume fraction of the dispersed phase in the pseudo-insert phase, ϕ is the volume fraction of the dispersed phase and ϕ_I is the volume fraction of the interphase. Moore et al. [96] showed

that ϕ_s can be taken as 0.5 for zeolites and 0.68 for carbon molecular sieves and β^* can be chosen close to 3 although the results were not found to be very sensitive to the value of β^* for the case of zeolite 4A/PVAc MMMs. We used ϕ_s as 0.68 and β^* as 3 following Shimekit et al. [33] and Moore et al. [96] in modified Maxwell model. Yilmaz and Keskin [50] recently showed that values of β^* and ϕ_s do not significantly affect the permeability results for MOF and ZIF-based MMMs. In order to determine which model gives the best permeability predictions compared to the experiments, average absolute relative error (AARE%) was calculated using Eq. (3.18):

$$\mathrm{AARE}(\%) = \frac{100}{N}\sum_{i=1}^{N}\left|\frac{p_i^{cal} - p_i^{exp}}{p_i^{exp}}\right| \tag{3.18}$$

In this equation, p_i^{cal} is the gas permeability calculated by theoretical permeation model, p_i^{exp} is the permeability measured in experiments and N is the number of data points. Maxwell model gave lower AARE% values both for CO_2 and N_2 permeability of Cd-6F/6FDA-DAM, ZIF-71/6FDA-Durene, ZIF-8/6FDA-Durene, CuBTC/Ultem and CuTPA/Ultem MMMs compared to the modified Maxwell model. Therefore, we used Maxwell model in calculating gas permeability of new PCN-based MMMs throughout this work. Calculated AARE% values for Maxwell and modified Maxwell model with two different ϕ_s values are given in Appendix A.

Chapter 4

RESULTS and DISCUSSIONS

4.1 Validation of the computational results

In order to validate the accuracy of our computational approach, we first predicted gas permeability of MOF and ZIF-based MMMs for which experimental gas permeability data are available. Figure 4.1 compares our gas permeability predictions from

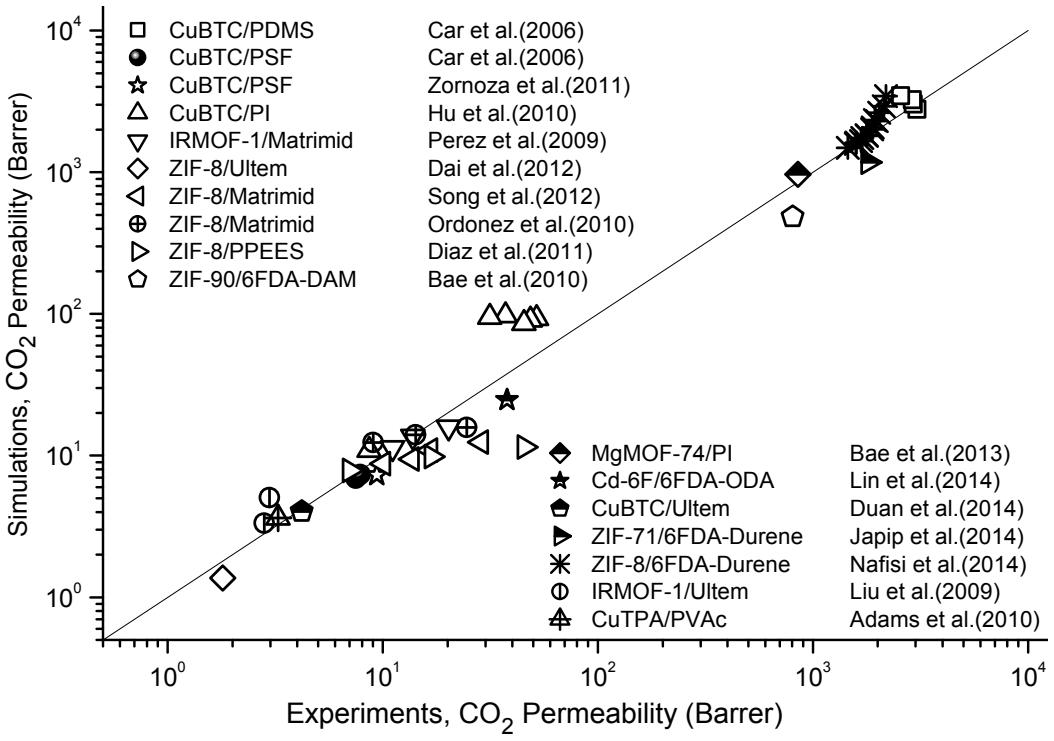

Figure 4.1 Comparison of molecular simulation results with experimentally measured CO_2 permeability of MOF and ZIF-based MMMs.

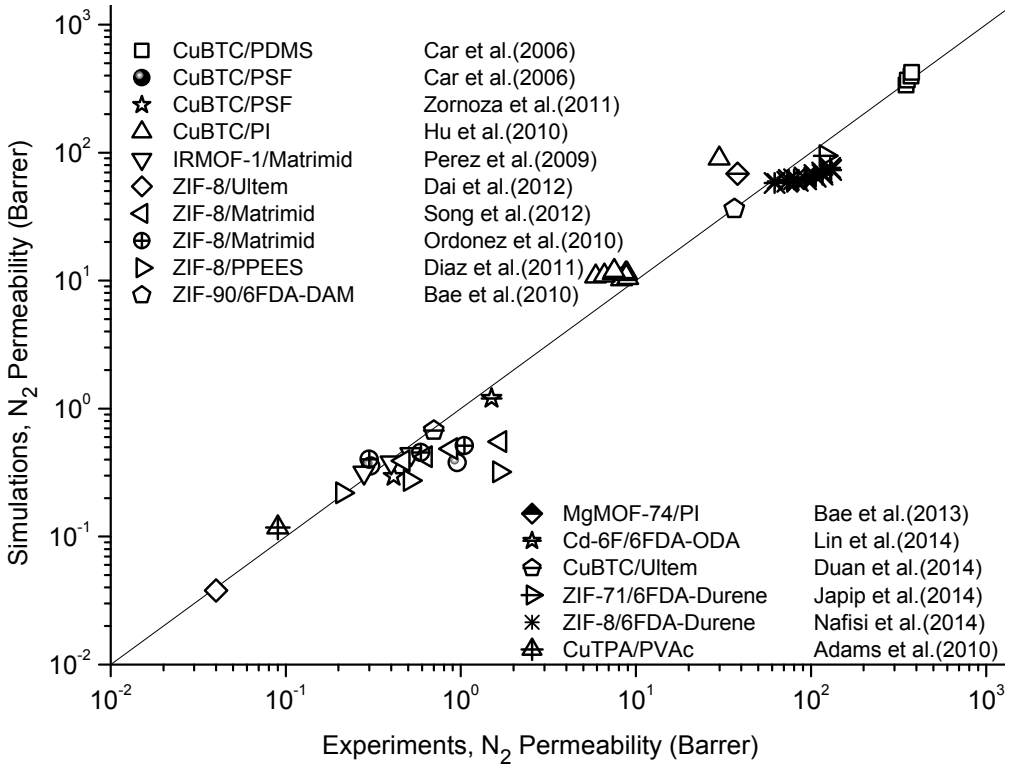

Figure 4.2 Comparison of molecular simulation results with experimentally measured N_2 permeability of MOF and ZIF-based MMMs.

molecular simulations with the experimentally measured results for various MOF and ZIF-based MMMs for CO_2 and Figure 4.2 for N_2. We collected 98 experimental data points from the literature for CO_2 and N_2 permeability of 15 different types of MOF and ZIF-based MMMs. The comparisons for gas permeabilities of CuBTC/PDMS, CuBTC/PSF, CuBTC/PI, IRMOF-1/Matrimid, ZIF-8/Ultem, ZIF-8/Matrimid, ZIF-8/PPEES, ZIF-90/6FDA-DAM, IRMOF-1/Ultem MMMs were taken from previous works [49, 50] whereas comparisons for gas permeabilities of MgMOF-74/PI, Cd-6F/6FDA-ODA, CuBTC/Ultem, ZIF-71/6FDA-Durene, ZIF-8/6FDA-Durene and CuTPA/PVAc MMMs were done for the first time in this thesis. Experimental permeability data of CuBTC/PSF

[60, 62] and ZIF-8/Matrimid [12, 67] MMMs were taken from two different research groups. Molecular simulations for these MOFs and ZIFs were carried out at the same temperature and pressure with the experiments to be consistent in making comparisons between experiments and simulations. Experimental conditions for the MMMs used in the validation of simulation results were as in the following: 308 K and 3.5 bar for CuBTC/Ultem [47] and ZIF-71/6FDA-Durene Pristine MMMs,[44] 308 K and 0.09 bar, 308 K and 4.48 bar for CO_2 and N_2, respectively, for CuTPA/PVAc MMM,[30] 298 K and 2 bar, 298K and 6 bar for ZIF-8/6FDA-Durene MMM,[45] 298 K and 2 bar for Mg-MOF-74/PI [43] and Cd-6F/6FDA-ODA MMMs.[46] Experimental conditions for remaining MMMs shown in Figure 4.1 and 4.2 can be found in the previous work of Yilmaz and Keskin [50]. The volume fraction of fillers in MMMs shown in Figure 4.1 and 4.2 ranged from 0.04 to 0.44.

Figure 4.1 and 4.2 showed that predictions of Maxwell model were in a good agreement with the experimental measurements of CO_2 and N_2 permeability especially for MMMs having low volume fraction of fillers. The maximum per cent error between the simulations and experiments was observed for CO_2 permeability of CuBTC/PI MMM. Simulations predicted higher CO_2 and N_2 permeabilities for CuBTC/PI MMMs compared to experiments [50]. This was explained by Hu et al. [61] who reported that their experimentally measured gas permeabilities are lower than expected due to the limited penetration of CO_2 and N_2 through the pores of CuBTC that are blocked by polymer chains and rigidification of the polymer. The minimum per cent error was calculated as 0.29% for N_2 permeability of ZIF-90/6FDA-DAM and 0.53% for CO_2 permeability of ZIF-8/6FDA-Durene. The good agreement between simulation results and experiments suggested that it is reasonable to use Maxwell model for estimating separation performance of new PCN-based MMMs for which experimental gas permeability data are not available.

4.2 Membrane properties of new PCN-based MMMs

After showing the good agreement between experiments and our predictions for gas permeability of various MOF and ZIF based MMMs, we used the same modelling approach to predict gas permeability and selectivity of new PCN-based MMMs which have not been fabricated to date. Calculation of the gas separation performance of PCN-based MMMs with theoretical models requires gas permeability data of pure polymers and PCNs. Gas permeability of polymers were obtained from the literature whereas gas permeability of pure PCNs were calculated as discussed in Chapter 3. Gas permeability of polymers is shown in Table 4.1.

Table 4.1 Permeability and selectivity of pure polymers

Polymer	P_{CO_2} (Barrer)	P_{N_2} (Barrer)	S_{CO_2/N_2}	Reference
Matrimid	9.00	0.25	36.00	[64]
Ultem	1.40	0.06	25.00	[66]
6FDA-DAM	842.41	54.99	15.32	[68]
Polyimide	45.00	1.27	35.43	[69]
MEEP	250.00	4.00	62.50	[70]
PIM-1	2300.00	92.00	25.00	[71]
PIM-7	1100.00	42.00	26.19	[71]
modified PDMS	2000.00	58.50	34.19	[72]
PTMGP	14000.00	1000.00	14.00	[73]
PTMSP	29000.00	2700.00	10.74	[73]

Permeability of polymers were obtained from the literature at the following pressures and temperatures: Matrimid,[64] Ultem,[66] and Polyimide[69] at 308 K, 2 bar, 6FDA-DAM [68] at 308 K, 7 bar, MEEP [70] at 303 K, 2 bar, PIM-1 [71] and PIM-7 [71] at 303 K, 0.2 bar, modified PDMS [72] at 308 K, 3 bar, PTMGP [73] and PTMSP [73] at 298 K.

As discussed in Chapter 3, adsorption amounts of CO_2 and N_2 were calculated with GCMC simulations. These results were later used in EMD simulations to obtain the diffusivity coefficients of CO_2 and N_2 in PCNs. Permeability of CO_2 and N_2 were then calculated based on flux as shown in Equation 3.5 and 3.6 and given in the units of Barrer as shown in Equation 3.7. The ratio of CO_2 permeability to N_2 permeability was used to calculate ideal selectivity as shown in Equation 3.8. Permeability and selectivity results for all 20 PCNs are given in Table 4.2. Permeability and selectivity of PCNs were also plotted in Figure 4.3 to show performances of PCN membranes in CO_2/N_2 separations with respect to Robeson's upper bound.

Table 4.2 Permeability and selectivity results for PCNs

MOF	P_{CO_2} (Barrer)	P_{N_2} (Barrer)	S_{CO_2/N_2}
PCN-6	317185.44	125559.38	2.53
PCN-6′	323639.75	233876.17	1.38
PCN-9-Co	134609.64	90849.50	1.48
PCN-9-Fe	21121.69	36987.99	0.57
PCN-9-Mn	98907.55	88042.74	1.12
PCN-10	190059.63	4067.36	46.73
PCN-11	670306.16	15168.47	44.19
PCN-13	461851.35	347625.67	1.33
PCN-14	941364.09	151131.37	6.23
PCN-16	481696.06	76076.57	6.33
PCN-16′	971322.50	826639.11	1.18
PCN-18	651700.96	58091.22	11.22
PCN-19	695656.60	210447.51	3.31
PCN-20	355580.01	120231.91	2.96
PCN-26	361769.52	148828.51	2.43
PCN-39	66606.81	65326.40	1.02
PCN-46	810373.35	287597.37	2.82
PCN-80	350513.16	197993.60	1.77
PCN-131′	10536.73	173.64	60.68
PCN-224-Ni	345168.38	152921.45	2.26

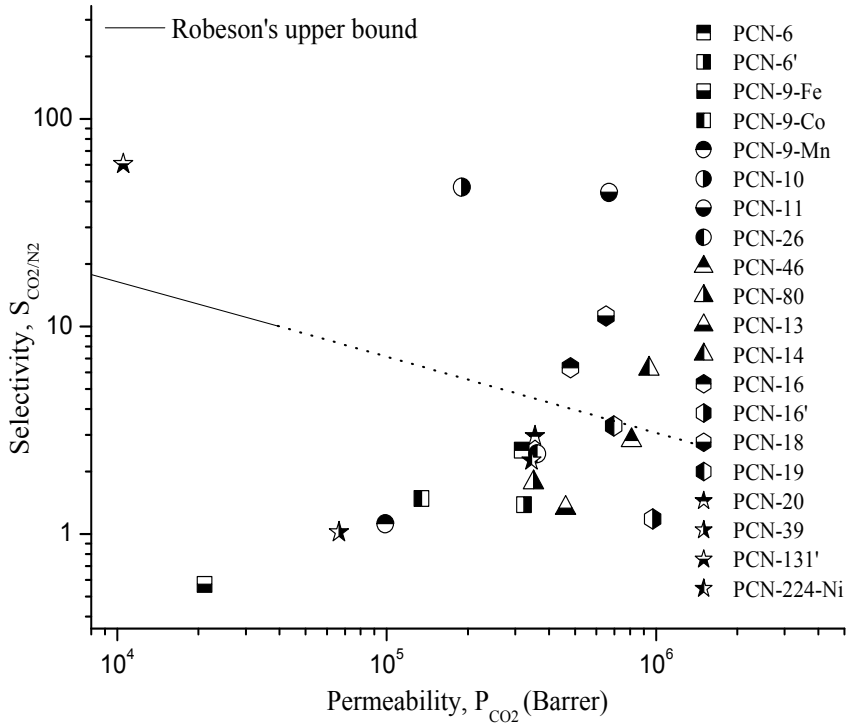

Figure 4.3 Permeability and selectivity results for PCNs with respect to Robeson's upper bound.

As shown in Figure 4.3, six PCNs, PCN-14, PCN-16, PCN-18, PCN-10, PCN-11 and PCN-131', overcame Robeson's upper bound due to their high permeability and/or selectivity, therefore these PCNs were expected to show an improved performance when used as fillers in MMMs with the polymers. Following the determination of gas permeability of pure PCNs and pure polymers, gas separation performance of PCN-based MMMs were calculated. Figures 4.4, 4.5, 4.6 represent predictions of molecular simulations for CO_2/N_2 selectivity and CO_2 permeability of 200 different PCN-based MMMs composed of 10 different polymers and 20 different PCNs.

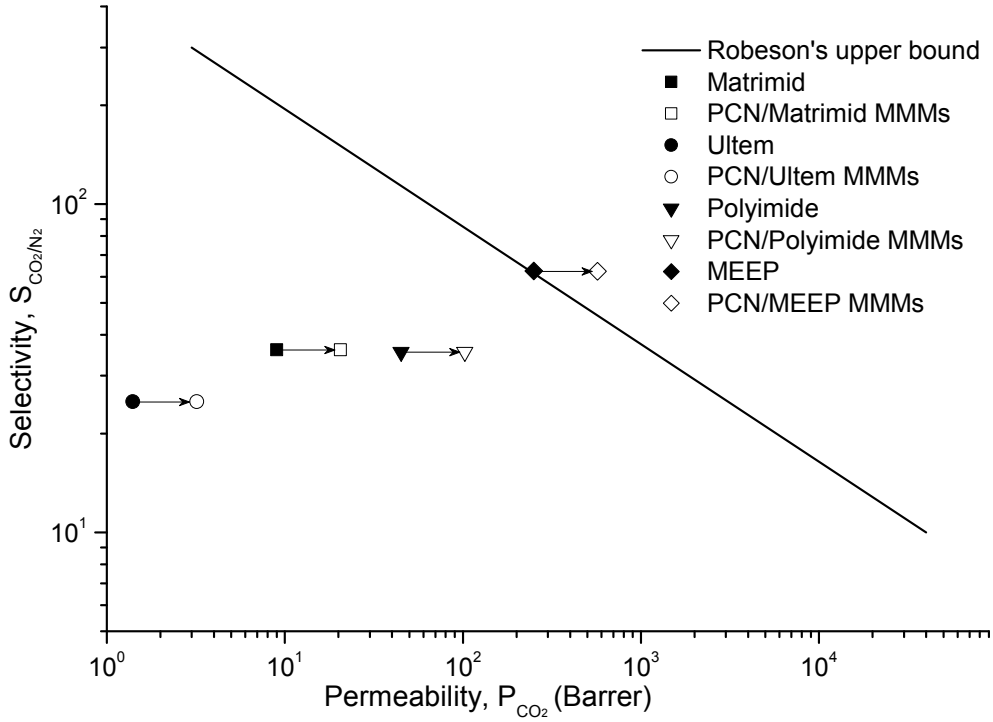

Figure 4.4 Predicted CO_2/N_2 selectivity and CO_2 permeability of PCN-based MMMs composed of polymers Matrimid, Ultem, Polyimide and MEEP. Filled symbols represent pure polymers and open symbols represent MMMs of the corresponding polymer. All MMM simulations were done under 298 K and 2 bar. All MMMs contain 0.3 volume fraction of PCN.

Maxwell model was used in permeability calculations and all calculations were done at 298 K and at a feed (permeate) pressure of 2 bar (vacuum) when the volume fraction of PCN was 0.3 in the membrane. Figure 4.4 shows that adding PCNs as filler particles into polymers Matrimid, Ultem, polyimide and MEEP increased the CO_2 permeability of these polymers but there was no change in CO_2/N_2 selectivity of these polymers. The selectivities of 10 PCNs considered in this work range from 0.57 to 60.7 and selectivities of polymers

Matrimid, Ultem, polyimide and MEEP range from 25 to 62.5. The selectivities of all PCNs are less than the selectivity of MEEP (62.5) therefore it was not possible to improve the selectivity of MEEP by incorporating PCNs as fillers into this polymer. The PCNs with the highest CO_2/N_2 selectivities were PCN-10 (46.7), PCN-11 (44.2) and PCN-131' (60.7), which all has higher selectivity than Matrimid (36), Ultem (25) and polyimide (35.4). However, selectivities of PCNs were not enough to enhance the selectivities of the polymers. CO_2 permeabilities of Matrimid, Ultem, polyimide and MEEP were enhanced by addition of PCNs into polymers since all the PCNs had higher CO_2 permeability (ranged from 10536 to 971322 Barrer) than the polymers (ranged from 1.4 to 250 Barrer). The high CO_2 permeability of PCNs is due to their highly porous structures. Results showed that gas permeabilities of different PCN-based MMMs were almost same, therefore a single symbol was used to represent different PCN-based MMMs for Matrimid, Ultem, polyimide and MEEP in Figure 4.4. In other words, the identity of PCN used as filler did not affect the performance of MMMs composed of these four polymers. For example, almost all PCNs improved the CO_2 permeability of Matrimid from 9 to 20.6 Barrer, permeability of Ultem from 1.4 to 3.2 Barrer, permeability of Polyimide from 45 to 102.8 Barrer and permeability of MEEP from 250 to 570 Barrer. One important result observed from Figure 4.4 was that PCN/MEEP MMMs overcame the upper bound established for CO_2/N_2 separation when any PCN with a volume fraction of 0.3 was used as fillers in the polymer due to the strong enhancement in CO_2 permeability.

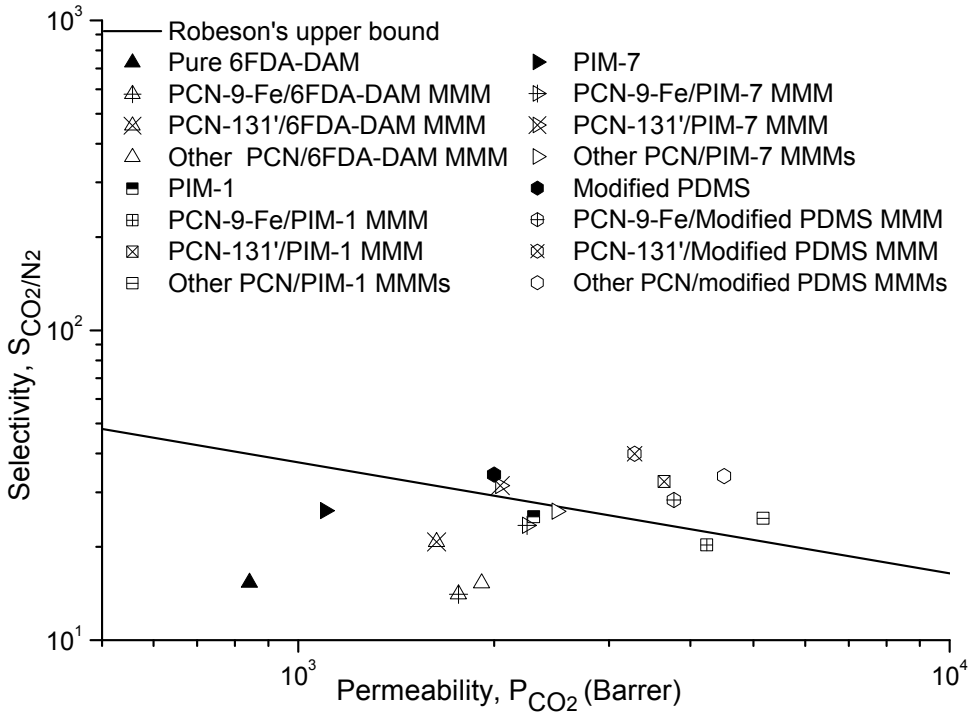

Figure 4.5 Predicted CO_2/N_2 selectivity and CO_2 permeability of PCN-based MMMs composed of polymers PIM-1, PIM-7, modified PDMS, 6FDA-DAM. Filled symbols represent pure polymers and open symbols represent MMMs of the corresponding polymer. All MMM simulations were done under 298 K and 2 bar. All MMMs contain 0.3 volume fraction of PCN.

Figure 4.5 shows that using PCNs as filler particles in 6FDA-DAM, PIM-1, PIM-7 and modified PDMS affected separation performances of these polymers in different ways:

(i) PCN-131' improved both the selectivity and permeability of 6FDA-DAM, PIM-1, PIM-7 and modified PDMS polymers. PCN-131' has a high CO_2 permeability (10536 Barrer) compared to these polymers (842, 2300, 1100, 2000 Barrer, respectively), therefore it enhanced CO_2 permeability of polymers. For example, CO_2 permeability of PIM-1 increased from 2300 to 4219 Barrer while its selectivity also increased from 25 to 35.2

when PCN-131' at a volume fraction of 0.3 was incorporated into the polymer. Similarly, CO_2 permeability of 6FDA-DAM increased from 842 to 1631 Barrer with a selectivity increase from 15.3 to 20.7. As a result, PCN-131' was a promising filler material that carried PIM-1 and PIM-7 over the upper bound due to the enhancement both in CO_2 permeability and CO_2/N_2 selectivity.

(ii) PCN-9-Fe increased CO_2 permeability of polymers at the expense of decreasing their CO_2/N_2 selectivity. This is due to the higher N_2 permeability of PCN-9-Fe (36988 Barrer) compared to its CO_2 permeability (21121 Barrer). This was the only PCN that show N_2 selective behavior due to slower CO_2 diffusion compared to other PCNs. For example, CO_2 permeability of modified PDMS increased from 2000 to 3775 Barrer while its CO_2/N_2 selectivity decreased from 34.2 to 28.3 when PCN-9-Fe at a volume fraction of 0.3 was incorporated into this polymer. Similarly, CO_2 permeability of PIM-7 increased from 1100 Barrer to 2244 Barrer at the expense of a decreased selectivity from 26.2 to 23.5 with PCN-9-Fe.

(iii) All other PCNs except PCN-9-Fe and PCN-131' enhanced CO_2 permeability of polymers without significantly changing their selectivity. The identity of the PCNs was not important since they all made the same improvement in CO_2 permeability. As a result, PIM-1 overcame the upper bound when combined with these PCNs due to a high increase in permeability and slight increase in selectivity. PIM-7-based MMMs were able to reach the upper bound but could not overcome it due to their unchanged selectivity. Modified PDMS is a polymer which was already over the upper bound and an improvement was observed only for CO_2 permeability when it was combined with these PCNs. The permeability of 6FDA-DAM was also improved with the addition of PCNs but it still could not overcome the upper bound.

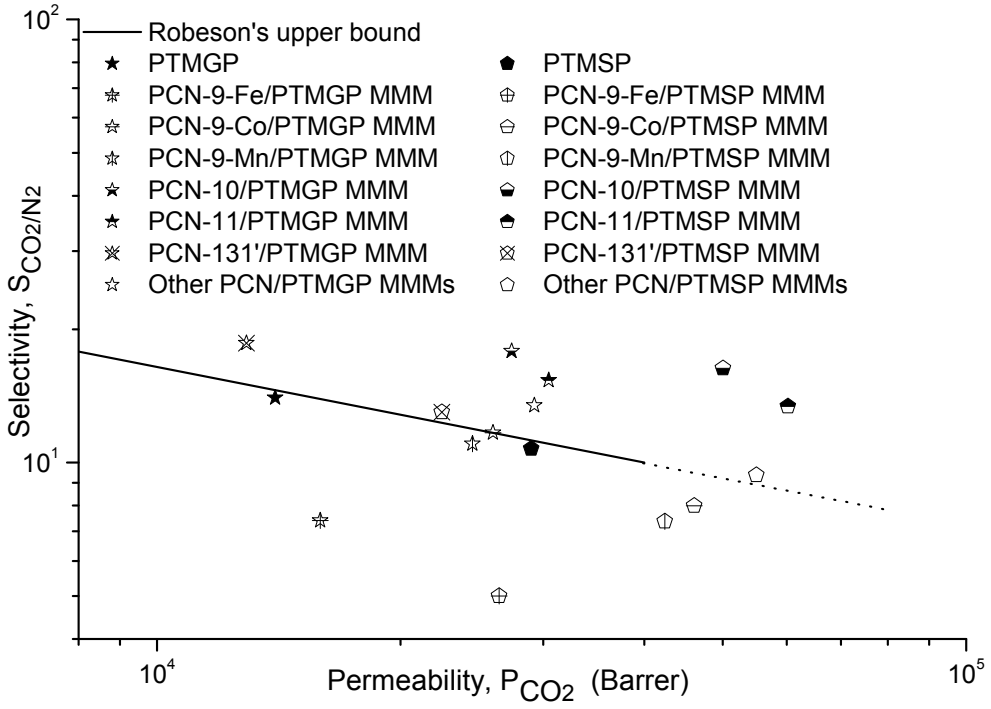

Figure 4.6 Predicted CO_2/N_2 selectivity and CO_2 permeability of PCN-based MMMs composed of polymers PTMGP and PTMSP. Filled symbols represent pure polymers and open symbols represent MMMs of the corresponding polymer. All MMM simulations were done under 298K and 2 bar. All MMMs contain 0.3 volume fraction of PCN.

PTMGP and PTMSP were the two polymers which had high CO_2 permeability (14000 and 29000 Barrer, respectively), but low CO_2/N_2 selectivity (14 and 10.74, respectively). They were located at the lower right end of the Robeson's upper bound as shown in Figure 4.6. The gas permeability of these two polymers were close to the permeability of most PCNs (ranges from 10536 to 971322 Barrer) compared to the permeability of other polymers (ranges from 1.4 to 2300 Barrer) considered in this work. Selectivity of these polymers (14 and 10.7, respectively) were higher than the selectivity of most PCNs (ranges from 0.57 to

11.2) and only lower than selectivity of PCN-10, PCN-11 and PCN-131' (46.7, 44.2 and 60.7, respectively). Because of this reason, MMMs composed of these polymers exhibited very different separation performances based on the identity of the PCNs used as fillers as seen in Figure 4.6. Below, we discuss the effects of using different PCNs (PCN-9-Fe, PCN-9-Co, PCN-9-Mn, PCN-10, PCN-11, PCN-131') as fillers in PTMGP and PTMSP.

(i) Increase in permeability and selectivity: PCN-10 (P_{CO_2}:190059 Barrer, S_{CO_2/N_2}:46.7) and PCN-11 (P_{CO_2}:670306 Barrer, S_{CO_2/N_2}:44.2) were the two materials that increased both the selectivity and permeability of the two polymers. For example, with PCN-10, the permeability of PTMGP increased from 14000 to 27425 Barrer and its selectivity increased from 14 to 17.9. Similarly, PTMSP exhibited a permeability increase from 29000 to 60233 Barrer and a selectivity increase from 10.7 to 13.4 when combined with PCN-11.

(ii) Increase in permeability and decrease in selectivity: PCN-9-Mn has similar permeabilities for CO_2 (98907 Barrer) and N_2 (88043 Barrer). Therefore, it is almost unselective (S_{CO_2/N_2}:1.1). The improvement in CO_2 permeability of PCNs occurred at the expense of a reduction in selectivity. For example, CO_2 permeability of PTMGP (PTMSP) increased from 14000 (29000) to 24546 (42422) Barrer while its selectivity decreased from 14 (10.7) to 11.0 (7.4) with addition of PCN-9-Mn fillers into polymer. Similarly, PCN-9-Co increased CO_2 permeability of polymers while decreasing their CO_2/N_2 selectivity. The decrease in selectivity was less pronounced compared to PCN-9-Mn.

(iii) Increase/decrease in permeability and decrease in selectivity: Since CO_2/N_2 selectivity of PCN-9-Fe (0.57) was lower than the selectivity of both polymers (14 and 10.7 for PTMGP and PTMSP, respectively), PCN-9-Fe decreased selectivity of both polymers. The CO_2 permeability of PCN-9-Fe (21122 Barrer) was higher than the permeability of PTMGP (14000 Barrer) but lower than the permeability of PTMSP (29000 Barrer).

Therefore, an increase (decrease) was observed in the CO_2 permeability of PTMGP (PTMSP) with PCN-9-Fe fillers.

(iv) Decrease in permeability and increase in selectivity: PCN-131' had a higher selectivity (60.7) but lower CO_2 permeability (10537 Barrer) than these two polymers. Using PCN-131' as fillers increased selectivity of both polymers while decreasing their permeability.

(v) Increase in permeability and no change in selectivity: PCNs other than mentioned above improved CO_2 permeability of these polymers but they did not significantly affect their selectivity. CO_2 permeability of PTMGP was 14000 Barrer. The highest permeability observed for PTMGP-based MMMs was 30938 Barrer with PCN-16' filler, while selectivity changed slightly from 14 to 13.6. For PTMSP, permeability increased from 29000 to 61941 Barrer with PCN-16' while selectivity changed slightly from 10.7 to 10.1.

All the permeability and selectivity data of 200 new PCN-based MMMs are given in the Appendix B. Results from Figures 4.4, 4.5, 4.6 suggested that PCN-10, PCN-11 and PCN-131' were the most promising filler candidates to improve separation performances of polymers.

4.3 Effect of PCN loading on the performance of PCN-based MMMs

In order to better evaluate potential of PCN-10, PCN-11 and PCN-131' as filler particles, we predicted gas permeability and selectivity of their MMMs as a function of filler’s volume fraction using Maxwell model. In this case, PCN’s volume fractions in MMMs were increased from 0.1 to 0.5. The effect of PCN loading on the performance of PCN-based MMMs were examined with considering the change in the position of the PCN-based MMM with respect to Robeson’s upper bound.

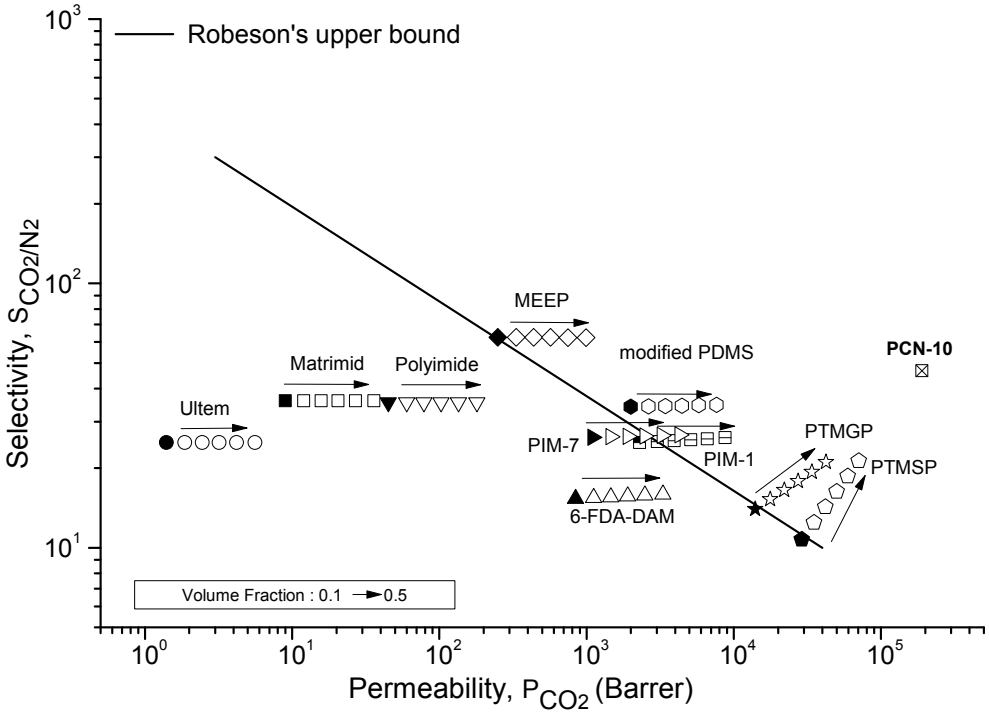

Figure 4.7 Predicted permeability and selectivity of PCN-10-based MMMs. Volume fraction of PCN-10 in MMMs was increased from 0.1 to 0.5.

Figure 4.7 illustrates separation performances of 50 new MMMs composed of 10 different polymers in which PCN-10 is used as filler particles in different volume fractions. Although PCN-10 had one of the highest CO_2/N_2 selectivity among all PCNs we studied in this thesis (46.7), it was able to significantly improve the selectivity of only two polymers, PTMGP and PTMSP. The selectivity of PTMGP increased from 14 to 21 and selectivity of PTMSP increased from 10.7 to 21.3 when PCN-10 at a volume fraction of 0.5 was incorporated into these polymers. The increase in selectivity of other polymers was not very high. For example, the selectivity of 6FDA-DAM increased from 15.3 to 15.9 and the selectivity of PIM-1 increased from 25 to 26 at the same volume fraction of PCN-10. When the volume fraction of PCN-10 was high, around 0.5, CO_2 permeability of MEEP, PIM-1,

PIM-7, PTMGP and PTMSP increased from 250, 2300, 1100, 14000, 29000 Barrer to 994, 8727, 4288, 42433 and 70819 Barrer, respectively. Overall, PCN-10 was able to carry MEEP, PIM-1, PIM-7, PTMGP and PTMSP over the Robeson's upper bound. While 0.1 volume fraction of PCN-10 was enough to carry MEEP, PIM-1, PTMGP and PTMSP over the upper bound, a volume fraction of 0.3 was required for PIM-7 to overcome the upper bound. In Figure 4.8, effect of filler volume fraction on another PCN, PCN-11-based MMMs is shown.

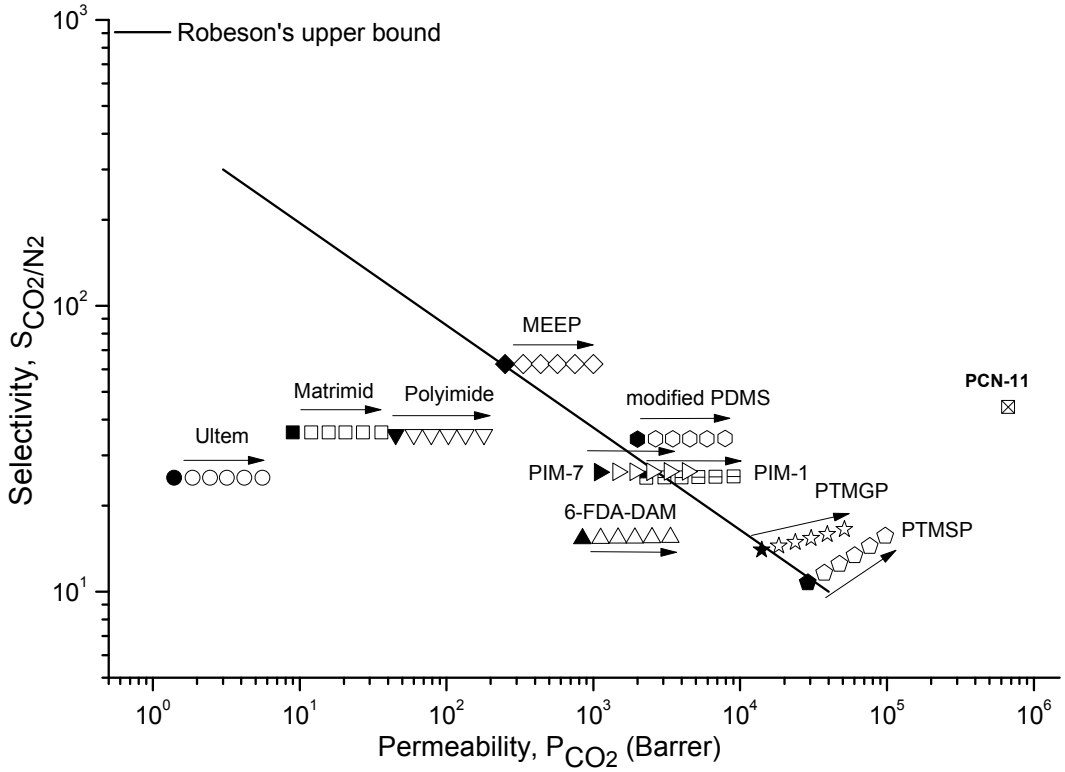

Figure 4.8 Predicted permeability and selectivity of PCN-11-based MMMs. Volume fraction of PCN-11 in MMMs was increased from 0.1 to 0.5.

Similar to PCN-10, PCN-11 increased permeability of polymers Ultem, Matrimid, polyimide, MEEP, PIM-1, PIM-7, 6FDA-DAM and modified PDMS without making a significant change in their selectivity as can be seen from Figure 4.8. Incorporating PCN-11 into PTMGP and PTMSP increased their selectivity from 14 to 16.5 and 10.7 to 15.7, respectively at a volume fraction of 0.5. As a result PCN-11 also carried MEEP, PIM-1, PIM-7, PTMGP and PTMSP over the upper bound by increasing either their selectivity or permeability. Last of all, In Figure 4.9, effect of filler volume fraction on PCN-131'-based MMMs is shown.

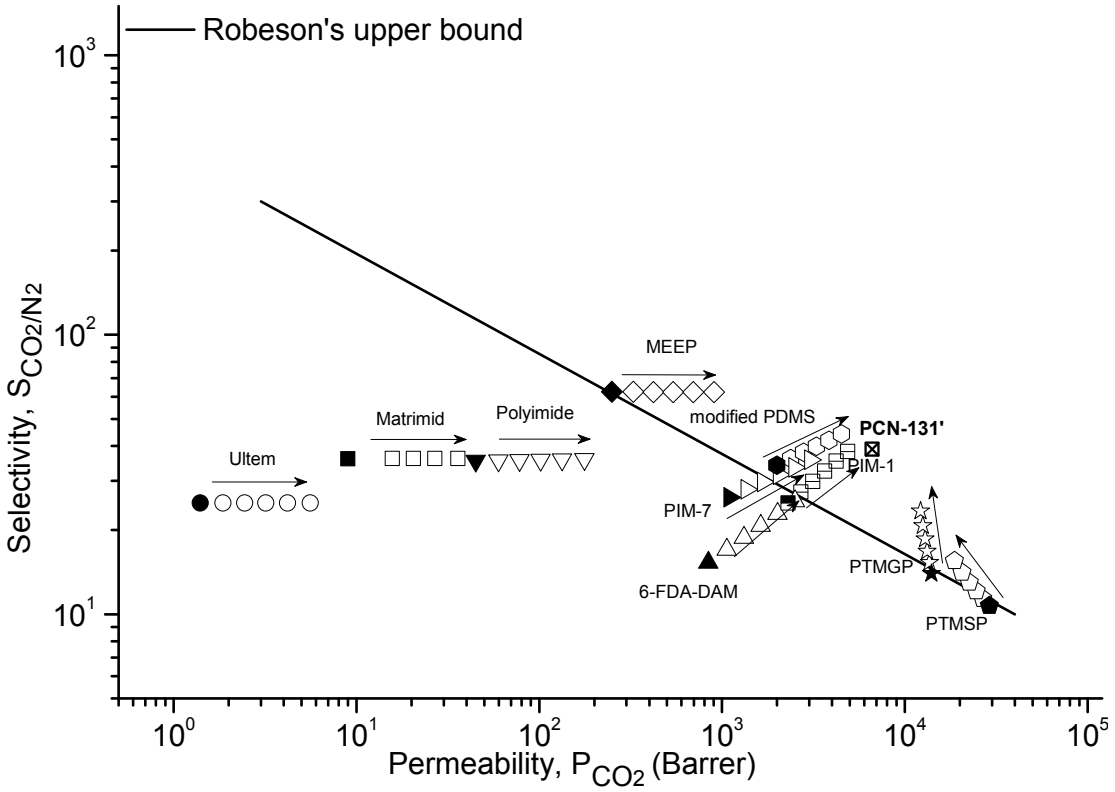

Figure 4.9 Predicted permeability and selectivity of PCN-131'-based MMMs. Volume fraction of PCN-131' in MMMs increases from 0.1 to 0.5.

Figure 4.9 shows that PCN-131' improved both the permeability and selectivity of the polymers PIM-1, PIM-7 and PTMGP. CO_2 permeability of PIM-1 increased from 2300 to 4879 Barrer while its selectivity increased from 25 to 38.3. CO_2 permeability of PIM-7 increased from 1100 to 3042 Barrer and its selectivity increased from 26.2 to 35.7 when PCN-131' was existing in the polymer at a volume fraction of 0.5. CO_2 permeability of MEEP increased from 250 to 904 Barrer at the expense of a very slight reduction in selectivity from 62.5 to 62.3. PCN-131' decreased CO_2 permeability of PTMGP from 14000 to 12194 Barrer but increased its selectivity from 14 to 23.4. Overall, PCN-131' was also identified as a promising filler to be used in MMMs which was able to carry several polymers such as MEEP, PIM-1, PIM-7, PTMGP and PTMSP over the Robeson's upper bound. PIM-7 required PCN at a volume fraction of 0.2 to overcome the upper bound while for MEEP, PIM-1, PTMGP and PTMSP a lower volume fraction (around 0.1) was sufficient.

4.4 Effect of PCN flexibility on the performance of PCN-based MMMs

In all molecular simulations discussed so far, we assumed that PCN framework is rigid. This is a good approximation to save computational time, however recent molecular simulations showed that framework flexibility may have significant effects on the diffusion properties of gas molecules in narrow-pored MOFs such as ZIF-8 [97, 98, 99, 100]. These simulation studies concluded that structure flexibility has negligible effect on the diffusion of small gas molecules in large pores but it may lead to large increases in diffusion of large gas molecules in MOFs having narrow pores. Haldoupis et al. [99] studied diffusion of H_2, He, Ar, CH_4 and Xe in ZIF-8 and reported that CH_4 (Xe) diffusivity in flexible ZIF-8 is 5 (13) orders of magnitude larger than the diffusivity calculated in rigid ZIF-8. Almost no change was observed in the diffusivity of H_2, He and Ar when flexibility of ZIF-8 was considered since kinetic diameters of these gas molecules are smaller than the pore diameter of ZIF-8. Hertäg et al. [100] showed that CH_4 diffusivity in flexible ZIF-8 is

significantly higher than the one in rigid structure. Recently, Yilmaz and Keskin [50] predicted separation performances of various ZIF-based MMMs considering the flexibility of the filler particles for the first time in the literature. Following their approach, we adapted three cases into this study: In Case 1, all simulations were performed based on rigid framework structures. In Case 2, it was assumed that flexibility only affects diffusivity of large molecules. Based on this assumption, diffusivity of N_2 in PCNs is increased 100 times. In Case 3, it was assumed that both N_2 and CO_2 diffusivities in PCNs are enhanced due to flexibility but the increase is more pronounced for the larger molecule, N_2 (100 times) and smaller for the other molecule, CO_2 (10 times). The reason for assigning a higher diffusivity to N_2 in flexible cases was that the kinetic diameter of N_2 (3.7 Å) is higher than that of CO_2 (3.3 Å) and it was expected to observe a more pronounced change in the diffusivity of N_2 in narrow-pored materials.

We first applied these cases to experimentally fabricated MMMs for which gas permeability data were available for comparison. In order to see, the effect of flexibility of MOF and ZIFs on the performance of MOF and ZIF- based MMMs, the AARE% (average absolute relative error) values were calculated using simulation results and experimental data as shown in Equation 3.18. The AARE% values for N_2 and CO_2 permeability of experimentally fabricated MMMs are given in Tables 4.3 and 4.4.

Table 4.3 AARE% values for N_2 permeability of MOF- and ZIF-based MMMs

MMM	P (bar)	T (K)	ϕ	P_{N_2} (Barrer) Case-1	AARE% Case-1	P_{N_2} (Barrer) Case-2	AARE% Case-2	P_{N_2} (Barrer) Case-3	AARE% Case-3	$P_{N_2,exp}$ (Barrer)	λ_{fp}
Cd-6F + 6FDA-ODA	2	308	0.07	0.96	35.72	0.96	35.72	0.96	35.72	1.50	600086
ZIF-71 + 6FDA-Durene	3.5	308	0.13	94.29	22.07	94.43	21.96	94.43	21.96	121.00	746.89
ZIF8 + 6FDA-Durene	2	298	0.07	61.06	18.26	70.77	5.26	70.77	5.26	74.70	2.03

ZIF8 + 6FDA-Durene			0.09	61.98	22.62	74.80	6.61	74.80	6.61	80.10	2.03
ZIF8 + 6FDA-Durene			0.13	63.86	30.44	83.42	9.13	83.42	9.13	91.80	2.03
ZIF8 + 6FDA-Durene			0.20	67.04	35.85	99.48	4.81	99.48	4.81	104.50	2.03
ZIF8 + 6FDA-Durene			0.25	69.73	39.83	114.67	1.06	114.67	1.06	115.90	2.03
ZIF8 + 6FDA-Durene			0.37	76.00	40.95	157.56	22.43	157.56	22.43	128.70	2.03
ZIF8 + 6FDA-Durene	6	298	0.04	57.88	6.50	63.12	1.96	63.12	1.96	61.90	1.98
ZIF8 + 6FDA-Durene			0.07	59.16	19.30	68.69	6.29	68.69	6.29	73.30	1.98
ZIF8 + 6FDA-Durene			0.09	60.02	28.63	72.60	13.67	72.60	13.67	84.10	1.98
ZIF8 + 6FDA-Durene			0.13	61.77	34.14	80.96	13.69	80.96	13.69	93.80	1.98
ZIF8 + 6 FDA-Durene			0.20	64.75	39.09	96.54	9.18	96.54	9.18	106.30	1.98
ZIF8 + 6FDA-Durene			0.25	67.26	42.27	111.28	4.48	111.28	4.48	116.50	1.98
ZIF8 + 6FDA-Durene			0.37	73.09	43.95	152.88	17.24	152.88	17.24	130.40	1.98
CuBTC + Ultem	3.5	308	0.44	0.67	4.08	0.67	4.08	0.67	4.08	0.70	993773
CuTPA + PVAc	4.48	308	0.14	0.12	30.65	0.12	30.65	0.12	30.65	0.09	2711161
CuBTC + PDMS	2	298	0.15	367.98	3.48	368.43	3.61	368.24	3.55	355.60	398.48
IRMOF-1 + Matrimid	2	308	0.34	0.38	5.07	0.38	5.07	0.38	5.07	0.40	508153
ZIF-8 + Matrimid	4	295	0.24	0.48	44.90	0.49	44.68	0.49	44.70	0.88	196.65
ZIF-90 + 6-FDA-DAM	2	298	0.19	36.68	0.29	36.68	0.29	36.68	0.30	36.57	66.65

Table 4.4. AARE% values for CO_2 permeability of MOF- and ZIF-based MMMs

MMM	**P (bar)**	**T(K)**	ϕ	P_{CO_2} **(Barrer) Case-1**	**AARE% Case-1**	P_{CO_2} **(Barrer) Case-2**	**AARE% Case-2**	P_{CO_2} **(Barrer) Case-3**	**AARE% Case-3**	$P_{CO_2,exp}$ **(Barrer)**	λ_{fp}
Cd-6F + 6FDA-	2	308	0.07	25.47	32.63	25.47	32.63	25.47	32.63	37.80	61423

ODA											
ZIF-71 + 6FDA-Durene	3.5	308	0.13	1176.80	34.80	1176.80	34.80	1357.92	24.77	1805.00	4.54
ZIF8 + 6FDA-Durene	2	298	0.07	1742.71	2.81	1742.71	2.81	1793.45	5.81	1695.00	16.49
ZIF8 + 6FDA-Durene			0.09	1827.51	3.05	1827.51	3.05	1895.36	6.87	1773.50	16.49
ZIF8 + 6FDA-Durene			0.13	2006.67	6.64	2006.67	6.64	2112.94	12.29	1881.70	16.49
ZIF8 + 6FDA-Durene			0.20	2333.70	20.27	2333.70	20.27	2518.23	29.78	1940.40	16.49
ZIF8 + 6FDA-Durene			0.25	2635.29	29.97	2635.29	29.97	2901.62	43.11	2027.60	16.49
ZIF8 + 6FDA-Durene			0.37	3447.08	57.72	3447.08	57.72	3982.27	82.21	2185.50	16.49
ZIF8 + 6FDA-Durene	6	298	0.04	1491.66	2.89	1491.66	2.89	1531.18	5.62	1449.70	9.77
ZIF8 + 6FDA-Durene			0.07	1591.25	0.53	1591.25	0.53	1664.25	5.15	1582.80	9.77
ZIF8 + 6FDA-Durene			0.09	1660.29	0.68	1660.29	0.68	1757.67	5.15	1671.60	9.77
ZIF8 + 6FDA-Durene			0.13	1805.21	1.46	1805.21	1.46	1956.97	9.99	1779.20	9.77
ZIF8 + 6 FDA-Durene			0.20	2066.45	9.16	2066.45	9.16	2327.54	22.95	1893.10	9.77
ZIF8 + 6FDA-Durene			0.25	2303.67	16.65	2303.67	16.65	2677.33	35.57	1974.90	9.77
ZIF8 + 6FDA-Durene			0.37	2925.17	36.99	2925.17	36.99	3659.23	71.37	2135.30	9.77
CuBTC + Ultem	3.5	308	0.44	4.03	4.08	4.03	4.08	4.03	4.08	4.20	427480
CuTPA + PVAc	4.48	308	0.14	3.63	11.40	3.63	11.40	3.63	11.40	3.26	656159
CuBTC + PDMS	2	298	0.15	3028.50	3.56	3028.50	3.56	3037.94	3.88	2924.44	156.62
IRMOF-1 + Matrimid	2	308	0.34	13.67	0.94	13.67	0.94	13.67	0.94	13.80	25913
ZIF-8 + Matrimid	4	295	0.24	10.91	34.40	10.91	34.40	10.91	34.40	16.63	2567.57
ZIF-90 + 6-FDA-DAM	2	298	0.19	485.24	39.69	485.24	39.69	510.24	36.58	804.53	10.88

Among these MOFs, ZIF-8 and ZIF-90 have narrow pores whereas all other MOFs have large pores. Limiting pore diameters of ZIF-8 (2.8/11.1 Å) and ZIF-90 (3.3/10.6 Å) are smaller than the kinetic diameter of N_2 whereas both narrow and large pores of other MOFs are larger than kinetic diameter of N_2 (6.4/12.8, 3.9/5.7, 4.1/4.9, 7.7/14.9, 5.8/7.3, 5.2/16.7 Å for CuBTC, CuTPA, Cd-6F, IRMOF-1, MgMOF-74, ZIF-71, respectively).[91] Information about structural properties of MOFs including pore diameters can be found in Table 4.5.

Table 4.5 Structural properties of the MOFs studied in this work

MOF	Density (g/cm^3)	Accesible surface area (m^2/g)	Pore Volume (cm^3/g)	LPD (Å)	LCD (Å)
PCN-6	0.584	3578.22	1.276	7.11	13.04
PCN-6′	0.292	5253.62	2.986	14.48	22.94
PCN-9-Co	0.859	1393.41	0.734	3.45	15.32
PCN-9-Fe	0.848	1265.06	0.735	3.03	15.31
PCN-9-Mn	0.842	1393.41	0.758	3.43	15.20
PCN-10	0.824	1888.22	0.820	3.08	10.51
PCN-11	0.804	2057.41	0.845	3.48	10.53
PCN-13	1.244	753.69	0.379	4.30	5.18
PCN-14	0.870	2049.94	0.723	4.48	6.66
PCN-16	0.771	2678.73	0.917	4.00	10.66
PCN-16′	0.818	2706.71	0.851	4.42	11.33
PCN-18	0.854	1552.48	0.672	4.31	6.63
PCN-19	1.000	1335.58	0.555	6.69	9.61
PCN-20	0.494	4185.31	1.594	9.13	16.65
PCN-26	0.895	2124.31	0.732	5.02	8.37

PCN-39	0.651	3227.67	1.029	4.53	7.55
PCN-46	0.663	3333.74	1.105	5.56	10.63
PCN-80	1.12	3566.07	0.65	6.44	12.69
PCN-131′	1.282	160.88	0.283	2.59	4.88
PCN-200	1.657	76.91	0.191	2.73	3.29
PCN-224-Ni	0.495	3419.42	1.641	13.64	23.98
IRMOF-1	0.593	3365.00	1.314	7.79	14.98
CuBTC	0.879	1916.94	0.801	6.07	12.74
ZIF-8	0.924	1332.95	0.582	2.80	11.16
ZIF-90	0.974	1306.10	0.614	3.30	10.62
CuTPA	1.25	553.67	0.420	3.25	5.72

Table 4.3 shows that AARE% values for N_2 permeability of flexible cases (Case 2 and Case 3) were almost same with the rigid case (Case 1) for CuBTC, CuTPA, Cd-6F, IRMOF-1, MgMOF-74, ZIF-71-based MMMs. The AARE% values for N_2 permeability of flexible cases were significantly lower than those of Case 1 for ZIF-8/6FDA-Durene MMMs. These results support the idea that considering flexibility of the filler particle plays an important role in predicting gas permeability of MMMs if the filler particle has a narrow pore diameter, close to the kinetic size of gas molecules. However, there are two exceptions to this conclusion, ZIF-8/Matrimid and ZIF-90/6FDA-DAM MMMs. Both ZIF-8 and ZIF-90 are narrow-pored materials but Table 4.3 shows that there was not a considerable change between the AARE% values of N_2 permeability for the rigid and flexible calculations of these MMMs. This can be explained with the following discussion. If the filler particle has a much higher gas permeability than the polymer ($\lambda_{fp} >> 1$ where λ_{fp} is the ratio of the gas permeability of the filler to the gas permeability of the polymer) and the

volume fraction of the filler is not very high ($\phi \leq 0.3$), then the Maxwell model (Eq. 3.11) becomes,

$$P = P_p \frac{(1+2\phi)}{(1-\phi)} \tag{4.1}$$

This means permeability of the MMM (P) depends only on the polymer's permeability (P_p) and the volume fraction of the filler, but not the filler's gas permeability. Under these conditions, the flexibility of the filler has no appreciable effect on the MMM's permeability. The ratio of filler's gas permeability to polymer's gas permeability (λ_{fp}) for each MMM are reported in Tables 4.3-4.4. The values of λ_{fp} (N_2) are 196.65 and 66.7 for ZIF-8/Matrimid and ZIF-90/6FDA-DAM MMMs, respectively. These values are high compared to λ_{fp} values of other ZIF-8-based MMMs which are all lower than 2. In other words, filler flexibility had no significant effect on the permeability of ZIF-8/Matrimid and ZIF-90/6FDA-DAM MMMs by Equation 4.1. These results indicated that not only the pore size of the MOF but also the ratio of MOF's gas permeability to polymer's gas permeability is an important factor determining the effect of flexibility on the MMM's performance.

In order to apply these cases to PCNs, first pore diameters of PCNs were need to be known and therefore calculated as discussed in Chapter 3.3. Based on the results discussed above, we applied three cases for PCNs which have limiting pore diameters that are close or less than the kinetic diameter of N_2. As shown in Table 4.5, among the PCNs we studied, PCN-9-Fe, PCN-10, PCN-11 and PCN-131' had narrow pore sizes (limiting pore diameters of 3.03, 3.08, 3.48, 2.59 Å, respectively [59]) for which we think flexibility would be significant for gas diffusivity.

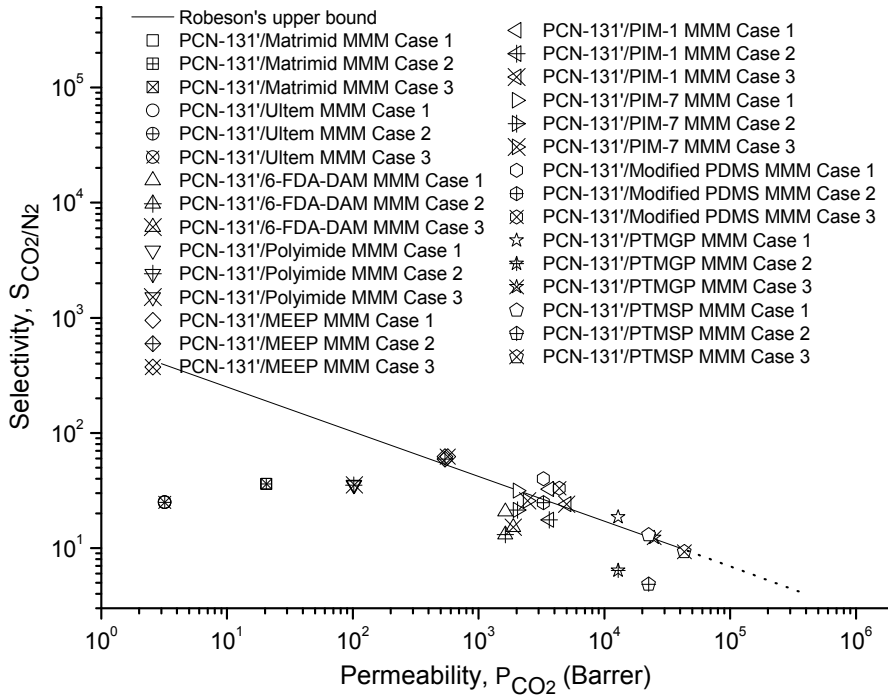

Figure 4.10 Change in CO_2 permeability and selectivity of PCN-131'-based MMMs when flexibility of the filler was considered.

Since PCN-131' has the smallest pore size, we investigated separation performances of PCN-131'-based MMMs when flexibility was taken into account in Figure 4.10. In these cases, volume fraction of PCN in polymer was again taken as 0.3 and all simulations were done under 298 K and 2 bar. According to Figure 4.10, permeability and selectivity of MMMs composed of Ultem, Matrimid, polyimide and MEEP were same in all cases indicating that flexibility did not affect the permeability and selectivity of membranes composed of these polymers.

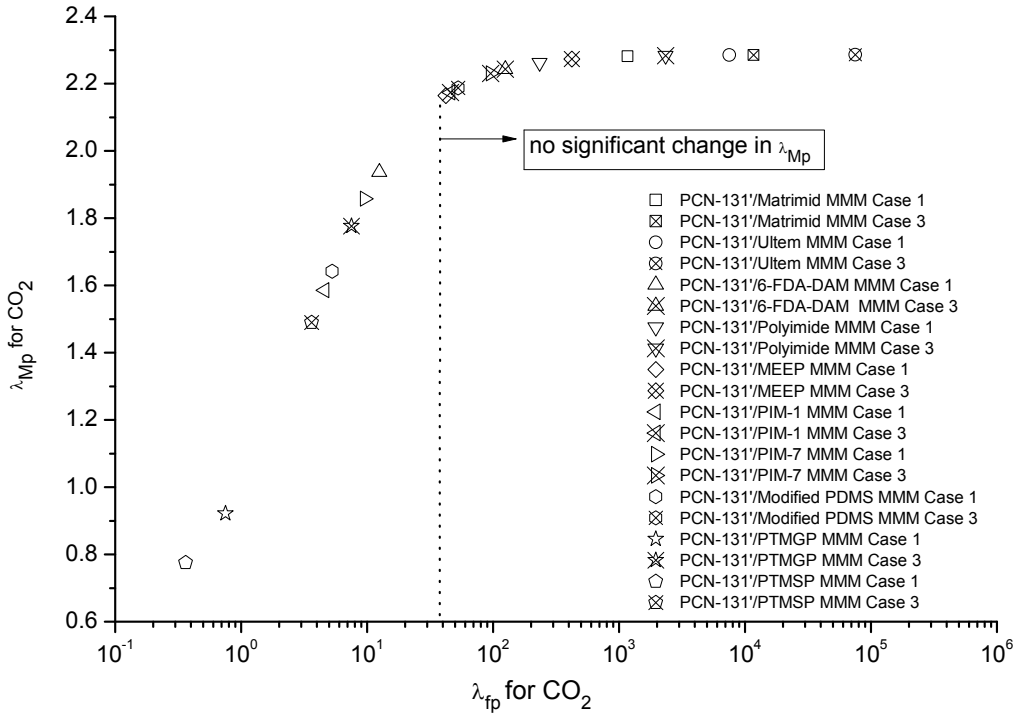

Figure 4.11 Change in CO_2 permeability of MMM vs. change in CO_2 permeability of filler (PCN-131'). CO_2 permeability is same for Case 1 and Case 2, therefore data for Case 2 are not shown.

This is due to the high λ_{fp} values (>>100) as can be seen from Figure 4.11 for CO_2. For example, CO_2 permeability of PCN-131' was 1170 times higher than permeability of Matrimid, therefore CO_2 permeability of PCN-131'/Matrimid MMM was equal to $2.28P_m$ at a filler volume fraction of 0.3 by Equation 4.1, independent from the filler's permeability and flexibility. The effect of flexibility can be clearly seen for MMMs composed of polymers 6FDA-DAM, PIM-1, PIM-7, modified PDMS, PTMGP and PTMSP in Figure 4.10. For example, CO_2 permeability (CO_2/N_2 selectivity) of PCN-131'/6FDA-DAM was 1631 Barrer (20.7) in Case 1 and 1889 Barrer (15.2) when flexibility of PCN was

considered in Case 3. Figure 4.11 shows that λ_{fp} was low, 12.5 for PCN-131'/6FDA-DAM in Case 1. When λ_{fp} was low, the filler had a more pronounced contribution to the permeability of the MMM. After a certain λ_{fp} value (greater than ~40 according to Figure 4.11), filler did not have a significant impact on the permeability of MMM.

Figure 4.10 shows that PTMGP and PTMSP-based MMMs were more sensitive to case changes i.e. flexibility. For example, in Case 1, CO_2 permeability of PTMGP and PTMSP were closer to that of PCN-131' compared to other polymers. Therefore, their λ_{fp} values were low (0.75 and 0.36 for PTMGP and PTMSP, respectively) than the λ_{fp} values of other PCN-131'/polymer membranes (1170, 7526, 12.5, 234, 42, 4.5, 9.5, 5.3 for Matrimid, Ultem, 6FDA-DAM, Polyimide, MEEP, PIM-1, PIM-7 and modified PDMS, respectively). The λ_{Mp} values for PCN-131'/PTMGP and PCN-131'/PTMSP MMMs were also lower (0.92 and 0.77, respectively) than other systems (ranges from 1.64 to 2.28). In Case 3, λ_{fp} values increased 10 times and λ_{Mp} values increased almost 2 times (1.77 and 1.49 for PTMGP and PTMSP, respectively) while it were almost same for other PCN-131'/polymer MMMs (ranges from 2.2 and 2.3). Therefore, using Case 1 (not considering filler's flexibility) or Case 3 (considering filler's flexibility) affected the performance of PTMGP and PTMSP-based MMMs more strongly than other polymers. This result can also be seen with considering the selectivity of PCN-based MMMs. As the selectivity of PCN-based MMMs is the ratio of CO_2 permeability to N_2 permeability, the effect of flexibility on CO_2 and N_2 permeability of PCN-based MMM reflected on the selectivity of the PCN-based MMM. For example, in Figure 4.10, it is seen that the change in selectivity of the PCN-based MMM was not considerable for Ultem, Matrimid, polyimide and MEEP based MMMs, more observable for 6FDA-DAM, PIM-1, PIM-7 and modified PDMS MMMs, but was the most significant in the case of PTMGP and PTMSP based MMMs.

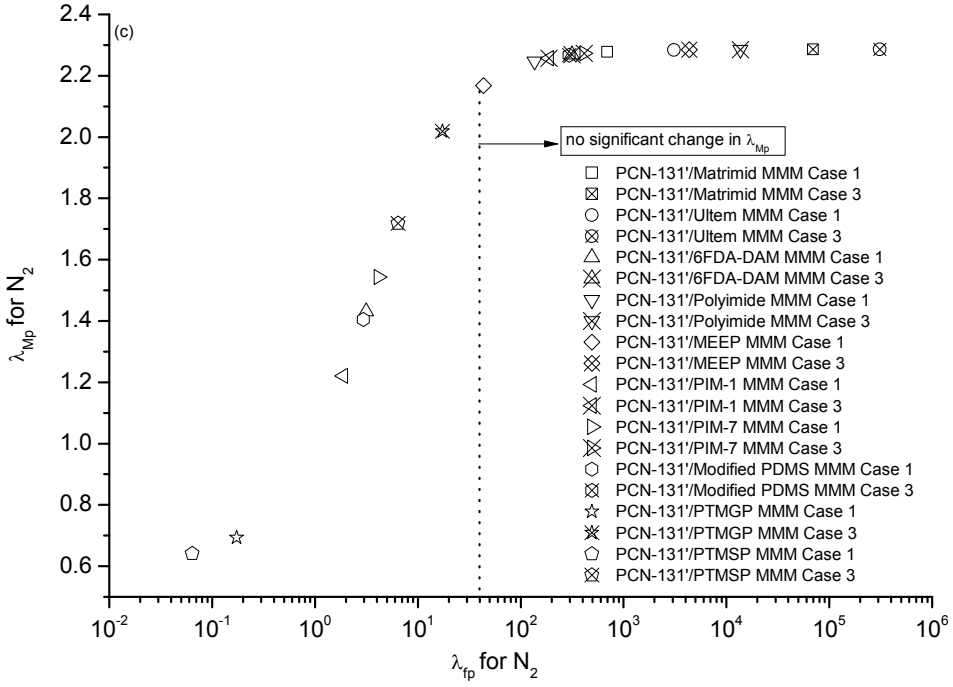

Figure 4.12 Change in N_2 permeability of MMM vs. change in N_2 permeability of filler (PCN-131'). N_2 permeability is same for Case 2 and Case 3, therefore data for Case 2 are not shown.

Similar to Figure 4.11 for CO_2, Figure 4.12 for N_2 shows that the lowest λ_{fp} are again for PCN-131'/PTMGP and PCN-131'/PTMSP MMMs and the change in λ_{Mp} value of these MMMs were more than the change in λ_{Mp} value of other PCN-based MMMs between Case 1 and Case 3. For example, the ratio of λ_{Mp} between Case 1 and Case 3 for PCN-131'/PTMGP was almost 3 while for other PCN-based MMMs it was around 1.5. As both CO_2 permeability and N_2 permeability of these MMMs were affected more than the other PCN-based MMMs, the changes in their selectivity were more significant. Similar results for PCN-9-Fe, PCN-10, PCN-11-based MMMs are shown in Appendix C.

Chapter 5

CONCLUSIONS

CO_2 capture from flue gas is an environmentally important process due to the impact of gaseous CO_2 on global warming. In this thesis, CO_2/N_2 separation performances of 200 different MMMs in which PCNs were used as fillers were examined combining molecular simulations and theoretical permeation models. Since there was no experimental data in the literature about gas permeability and selectivity of PCN-based MMMs, validation of our computational method was done by comparing simulation results with experimentally reported gas permeability and selectivity data of various MOF and ZIF-based MMMs. Motivated from the good agreement between experiments and simulations, we applied our methodology to 200 new PCN-based MMMs, which have not been fabricated yet. Using PCNs as filler particles in MMMs improved both CO_2 and N_2 permeability of the polymers. CO_2/N_2 selectivity of polymers increased when PCN-10, PCN-11 and PCN-131' were used as fillers. These three PCNs were identified as the most promising ones since several polymers could exceed the Robeson's upper bound established for CO_2/N_2 separation when PCN-10, PCN-11 and PCN-131' were used as filler particles. We also investigated the effect of PCN flexibility on the permeability and selectivity of MMMs and concluded that flexibility must be considered if the pore size of the PCN is close to the kinetic diameter of gas molecule and the ratio of permeability of PCN to permeability of polymer is low. For rapid computational screening of PCN/polymer MMMs using molecular simulations as suggested in this work, flexibility of the fillers can be neglected as a reasonable

approximation if the filler volume fraction is less than 0.3 and if the filler is much more permeable than the polymer.

In this thesis, the interaction of PCNs with water molecules and other impurities in flue gas was not investigated. Keskin et al. [101] and Ding et al. [102] emphasized the importance of investigating the effect of water vapor and flue gas impurities on stability of MOFs and CO_2 adsorption in MOFs. Similarly, the stability and adsorbent properties of PCNs have to be investigated in detail under these specified conditions before deciding on their applicability for membrane-based separations in the future. Also, the MMM model, Maxwell model, used in this study assumes that the polymer phase and the inorganic phase are compatible to each other to be combined as a one phase membrane, however, the homogeneity of the interface between the polymer phase and the PCN phase will be observable only with experimental work. Last but not the least, the effect of PCN flexibility on CO_2 and N_2 diffusion is hypothetically studied in this thesis. Detailed simulations about PCN flexibility would offer more insight about these effects.

BIBLIOGRAPHY

[1] Root TL, Price JT, Hall KR, Schneider SH, Rosenzweig C, Pounds JA. Fingerprints of global warming on wild animals and plants. Nature. 2003;421:57-60.
[2] Aaron D, Tsouris C. Separation of CO_2 from Flue Gas: A Review. Separation Science and Technology. 2005;40:321-348.
[3] Veawab A, Aroonwilas A, Chakma A, Tontiwachwuthikul P, Solvent formulation for CO2 separation from flue gas streams. 2001: Publisher.
[4] Koros WJ, Mahajan R. Pushing the limits on possibilities for large scale gas separation: which strategies? Journal of Membrane Science. 2000;175:181-196.
[5] Khalilpour R, Mumford K, Zhai H, Abbas A, Stevens G, Rubin ES. Membrane-based carbon capture from flue gas: a review. Journal of Cleaner Production. 2014.
[6] Robeson LM. Correlation of separation factor versus permeability for polymeric membranes. Journal of Membrane Science. 1991;62:165-185.
[7] Robeson LM. The upper bound revisited. Journal of Membrane Science. 2008;320:390-400.
[8] Husain S, Koros WJ. Mixed matrix hollow fiber membranes made with modified HSSZ-13 zeolite in polyetherimide polymer matrix for gas separation. Journal of Membrane Science. 2007;288:195-207.
[9] Bakhtiari O, Mosleh S, Khosravi T, Mohammadi T. Synthesis and characterization of polyimide mixed matrix membranes. Separation Science and Technology. 2011;46:2138-2147.
[10] Kim S, Pechar TW, Marand E. Poly(imide siloxane) and carbon nanotube mixed matrix membranes for gas separation. Desalination. 2006;192:330-339.
[11] Bae TH, Lee JS, Qiu WL, Koros WJ, Jones CW, Nair S. A high-performance gas-separation membrane containing submicrometer-sized metal-organic framework crystals. Angewandte Chemie International Edition. 2010;49:9863-9866.
[12] Ordoñez MJC, Balkus Jr KJ, Ferraris JP, Musselman IH. Molecular sieving realized with ZIF-8/Matrimid® mixed-matrix membranes. Journal of Membrane Science. 2010;361:28-37.
[13] Vu DQ, Koros WJ, Miller SJ. Mixed matrix membranes using carbon molecular sieves - I. preparation and experimental results. Journal of Membrane Science. 2003;211:311-334.
[14] Zhang YF, Musseman IH, Ferraris JP, Balkus KJ. Gas permeability properties of Matrimid® membranes containing the metal-organic framework Cu-BPY-HFS. Journal of Membrane Science. 2008;313:170-181.
[15] Basu S, Cano-Odena A, Vankelecom IFJ. Asymmetric Matrimid®/$[Cu_3(BTC)_2]$ mixed-matrix membranes for gas separations. Journal of Membrane Science. 2010;362:478-487.
[16] Banerjee R, Phan A, Wang B, Knobler C, Furukawa H, O'Keeffe M, Yaghi OM. High-throughput synthesis of zeolitic imidazolate frameworks and application to CO_2 capture. Science. 2008;319:939-943.
[17] Yaghi OM, O'Keeffe M, Ockwig NW, Chae HK, Eddaoudi M, Kim J. Reticular synthesis and the design of new materials. Nature. 2003;423:705-714.

[18] Eddaoudi M, Kim J, Rosi N, Vodak D, Wachter J, O'Keeffe M, Yaghi OM. Systematic design of pore size and functionality in isoreticular MOFs and their application in methane storage. Science. 2002;295:469-472.
[19] Jiang JW. Molecular simulations in metal-organic frameworks for diverse potential applications. Molecular Simulation. 2014;40:516-536.
[20] Ma SQ, Simmons JM, Sun DF, Yuan DQ, Zhou HC. Porous metal-organic frameworks based on an anthracene derivative: syntheses, structure analysis, and hydrogen sorption studies. Inorganic Chemistry. 2009;48:5263-5268.
[21] Xiang Z, Cao D, Lan J, Wang W, Broom DP. Multiscale simulation and modelling of adsorptive processes for energy gas storage and carbon dioxide capture in porous coordination frameworks. Energy & Environmental Science. 2010;3:1469-1487.
[22] Frenkel D, Smit B. Understanding molecular simulation: from algorithms to applications. San Diego: Academic Press; 2002.
[23] Freeman BD. Basis of permeability/selectivity tradeoff relations in polymeric gas separation membranes. Macromolecules. 1999;32:375-380.
[24] Shah M, McCarthy MC, Sachdeva S, Lee AK, Jeong H-K. Current status of metal–organic framework membranes for gas separations: promises and challenges. Industrial & Engineering Chemistry Research. 2012;51:2179-2199.
[25] Jeazet HBT, Staudt C, Janiak C. Metal-organic frameworks in mixed-matrix membranes for gas separation. Dalton Transactions. 2012;41:14003-14027.
[26] Erucar I, Keskin S. Molecular Modeling of MOF-based Mixed Matrix Membranes. Current Organic Chemistry. 2014;18:2364-2380.
[27] Kulprathipanja S. Mixed matrix membrane development. Annals of the New York Academy of Sciences. 2003;984:361-369.
[28] Baker RW, Low BT. Gas separation membrane materials: A perspective. Macromolecules. 2014;47:6999-7013.
[29] Shao L, Low BT, Chung T-S, Greenberg AR. Polymeric membranes for the hydrogen economy: contemporary approaches and prospects for the future. Journal of Membrane Science. 2009;327:18-31.
[30] Adams R, Carson C, Ward J, Tannenbaum R, Koros W. Metal organic framework mixed matrix membranes for gas separations. Microporous and Mesoporous Materials. 2010;131:13-20.
[31] Caro J. Are MOF membranes better in gas separation than those made of zeolites? Current Opinion in Chemical Engineering. 2011;1:77-83.
[32] Zornoza B, Tellez C, Coronas J, Gascon J, Kapteijn F. Metal organic framework based mixed matrix membranes: An increasingly important field of research with a large application potential. Microporous and Mesoporous Materials. 2013;166:67-78.
[33] Shimekit B, Mukhtar H, Murugesan T. Prediction of the relative permeability of gases in mixed matrix membranes. Journal of Membrane Science. 2011;373:152-159.
[34] Dong G, Li H, Chen V. Challenges and opportunities for mixed-matrix membranes for gas separation. Journal of Materials Chemistry A. 2013;1:4610-4630.

[35] Millward AR, Yaghi OM. Metal-organic frameworks with exceptionally high capacity for storage of carbon dioxide at room temperature. Journal of the American Chemical Society. 2005;127:17998-17999.
[36] Venna SR, Zhu M, Li S, Carreon MA. Knudsen diffusion through ZIF-8 membranes synthesized by secondary seeded growth. Journal of Porous Materials. 2014;21:235-240.
[37] Venna SR, Carreon MA. Metal organic framework membranes for carbon dioxide separation. Chemical Engineering Science. 2015;124:3-19.
[38] Caskey SR, Wong-Foy AG, Matzger AJ. Dramatic tuning of carbon dioxide uptake via metal substitution in a coordination polymer with cylindrical pores. Journal of the American Chemical Society. 2008;130:10870-10871.
[39] Liu Y, Zeng G, Pan Y, Lai Z. Synthesis of highly c-oriented ZIF-69 membranes by secondary growth and their gas permeation properties. Journal of Membrane Science. 2011;379:46-51.
[40] Guerrero VV, Yoo Y, McCarthy MC, Jeong H-K. HKUST-1 membranes on porous supports using secondary growth. Journal of Materials Chemistry. 2010;20:3938-3943.
[41] Yang Q, Xue C, Zhong C, Chen JF. Molecular simulation of separation of CO_2 from flue gases in CU-BTC metal-organic framework. AIChE journal. 2007;53:2832-2840.
[42] Zhang Z, Li Z, Li J. Computational Study of Adsorption and Separation of CO_2, CH_4, and N_2 by an rht-Type Metal–Organic Framework. Langmuir. 2012;28:12122-12133.
[43] Bae TH, Long JR. CO_2/N_2 separations with mixed-matrix membranes containing Mg_2(dobdc) nanocrystals. Energy and Environmental Science. 2013;6:3565-3569.
[44] Japip S, Wang H, Xiao YC, Chung TS. Highly permeable zeolitic imidazolate framework (ZIF)-71 nano-particles enhanced polyimide membranes for gas separation. Journal of Membrane Science. 2014;467:162-174.
[45] Nafisi V, Hagg MB. Gas separation properties of ZIF-8/6FDA-durene diamine mixed matrix membrane. Separation and Purification Technology. 2014;128:31-38.
[46] Lin RJ, Ge L, Hou L, Strounina E, Rudolph V, Zhu ZH. Mixed matrix membranes with strengthened MOFs/polymer interfacial interaction and improved membrane performance. Acs Applied Materials & Interfaces. 2014;6:5609-5618.
[47] Duan CJ, Kang GD, Liu DD, Wang LN, Jiang C, Cao YM, Yuan Q. Enhanced gas separation properties of metal organic frameworks/polyetherimide mixed matrix membranes. Journal of Applied Polymer Science. 2014;131:40719-40728.
[48] Basu S, Cano-Odena A, Vankelecom IF. MOF-containing mixed-matrix membranes for CO_2/CH_4 and CO_2/N_2 binary gas mixture separations. Separation and Purification Technology. 2011;81:31-40.
[49] Erucar I, Manz TA, Keskin S. Effects of electrostatic interactions on gas adsorption and permeability of MOF membranes. Molecular Simulation. 2014;40:557-570.
[50] Yilmaz G, Keskin S. Molecular modeling of MOF and ZIF-filled MMMs for CO_2/N_2 separations. Journal of Membrane Science. 2014;454:407-417.
[51] Ma S, Zhou H-C. A metal-organic framework with entatic metal centers exhibiting high gas adsorption affinity. Journal of the American Chemical Society. 2006;128:11734-11735.

[52] Lu W, Yuan D, Makal TA, Li JR, Zhou HC. A Highly Porous and Robust (3, 3, 4)-Connected Metal–Organic Framework Assembled with a 90° Bridging-Angle Embedded Octacarboxylate Ligand. Angewandte Chemie International Edition. 2012;51:1580-1584.
[53] Jiang HL, Feng DW, Liu TF, Li JR, Zhou HC. Pore surface engineering with controlled loadings of functional groups via click chemistry in highly stable metal-organic frameworks. Journal of the American Chemical Society. 2012;134:14690-14693.
[54] Zhuang WJ, Yuan DQ, Liu DH, Zhong CL, Li JR, Zhou HC. Robust metal-organic framework with an octatopic ligand for gas adsorption and separation: combined characterization by experiments and molecular simulation. Chemistry of Materials. 2012;24:18-25.
[55] Liu YY, Li JR, Verdegaal WM, Liu TF, Zhou HC. Isostructural metal-organic frameworks assembled from functionalized diisophthalate ligands through a ligand-truncation strategy. Chemistry-a European Journal. 2013;19:5637-5643.
[56] Liu YY, Chen YP, Liu TF, Yakovenko AA, Raiff AM, Zhou HC. Selective gas adsorption and unique phase transition properties in a stable magnesium metal-organic framework constructed from infinite metal chains. CrystEngComm. 2013;15:9688-9693.
[57] Babarao R, Jiang YQ, Medhekar NV. Postcombustion CO_2 capture in functionalized porous coordination networks. Journal of Physical Chemistry C. 2013;117:26976-26987.
[58] Ozturk TN, Keskin S. Predicting gas separation performances of porous coordination networks using atomistic simulations. Industrial and Engineering Chemistry Research. 2013;52:17627-17639.
[59] Ozturk TN, Keskin S. Computational screening of porous coordination networks for adsorption and membrane-based gas separations. Journal of Physical Chemistry C. 2014;118:13988-13997.
[60] Car A, Stropnik C, Peinemann K-V. Hybrid membrane materials with different metal–organic frameworks (MOFs) for gas separation. Desalination. 2006;200:424-426.
[61] Hu J, Cai H, Ren H, Wei Y, Xu Z, Liu H, Hu Y. Mixed-matrix membrane hollow fibers of $Cu_3(BTC)_2$ MOF and polyimide for gas separation and adsorption. Industrial and Engineering Chemistry Research. 2010;49:12605-12612.
[62] Zornoza B, Seoane B, Zamaro JM, Téllez C, Coronas J. Combination of MOFs and zeolites for mixed-matrix membranes. ChemPhysChem. 2011;12:2781-2785.
[63] Liu C, McCulloch B, Wilson ST, Benin AI, Schott ME, inventors; UOP LLC, assignee. Metal organic framework—polymer mixed matrix membranes. United States patent US 7,637,983. 2009 Dec 29.
[64] Perez EV, Balkus KJ, Ferraris JP, Musselman IH. Mixed-matrix membranes containing MOF-5 for gas separations. Journal of Membrane Science. 2009;328:165-173.
[65] Díaz K, López-González M, del Castillo LF, Riande E. Effect of zeolitic imidazolate frameworks on the gas transport performance of ZIF8-poly(1,4-phenylene ether-ether-sulfone) hybrid membranes. Journal of Membrane Science. 2011;383:206-213.
[66] Dai Y, Johnson JR, Karvan O, Sholl DS, Koros WJ. Ultem®/ZIF-8 mixed matrix hollow fiber membranes for CO_2/N_2 separations. Journal of Membrane Science. 2012;401–402:76-82.

[67] Song Q, Nataraj SK, Roussenova MV, Tan JC, Hughes DJ, Li W, Bourgoin P, Alam MA, Cheetham AK, Al-Muhtaseb SA, Sivaniah E. Zeolitic imidazolate framework (ZIF-8) based polymer nanocomposite membranes for gas separation. Energy & Environmental Science. 2012;5:8359-8369.
[68] Qiu WL, Xu LR, Chen CC, Paul DR, Koros WJ. Gas separation performance of 6FDA-based polyimides with different chemical structures. Polymer. 2013;54:6226-6235.
[69] Yang L, Fang J, Meichin N, Tanaka K, Kita H, Okamoto K. Gas permeation properties of thianthrene-5,5,10,10-tetraoxide-containing polyimides. Polymer. 2001;42:2021-2029.
[70] Orme CJ, Harrup MK, Luther TA, Lash RP, Houston KS, Weinkauf DH, Stewart FF. Characterization of gas transport in selected rubbery amorphous polyphosphazene membranes. Journal of Membrane Science. 2001;186:249-256.
[71] Budd PM, Msayib KJ, Tattershall CE, Ghanem BS, Reynolds KJ, McKeown NB, Fritsch D. Gas separation membranes from polymers of intrinsic microporosity. Journal of Membrane Science. 2005;251:263-269.
[72] Senthilkumar U, Reddy BSR. Polysiloxanes with pendent bulky groups having amino-hydroxy functionality: structure-permeability correlation. Journal of Membrane Science. 2007;292:72-79.
[73] Mizumoto T, Masuda T, Higashimura T. Polymerization of [o-(trimethylgermyl)phenyl]acetylene and polymer characterization. Journal of Polymer Science Part a-Polymer Chemistry. 1993;31:2555-2561.
[74] Smit B. Phase diagrams of Lennard-Jones fluids. Journal of Chemical Physics. 1992;96:8639-8640.
[75] Rappe AK, Casewit CJ, Colwell KS, Goddard WA, Skiff WM. UFF, a full periodic table force field for molecular mechanics and molecular dynamics simulations. Journal of the American Chemical Society. 1992;114:10024-10035.
[76] Mayo SL, Olafson BD, Goddard WA. Dreiding: a generic force field for molecular simulations. Journal of Physical Chemistry. 1990;94:8897-8909.
[77] Jorgensen WL, Tirado-Rives J. The OPLS [optimized potentials for liquid simulations] potential functions for proteins, energy minimizations for crystals of cyclic peptides and crambin. Journal of the American Chemical Society. 1988;110:1657-1666.
[78] Potoff JJ, Siepmann JI. Vapor-liquid equilibria of mixtures containing alkanes, carbon dioxide, and nitrogen. Aiche Journal. 2001;47:1676-1682.
[79] Makrodimitris K, Papadopoulos GK, Theodorou DN. Prediction of permeation properties of CO_2 and N_2 through silicalite via molecular simulations. Journal of Physical Chemistry B. 2001;105:777-788.
[80] Wilmer CE, Kim KC, Snurr RQ. An extended charge equilibration method. Journal of Physical Chemistry Letters. 2012;3:2506-2511.
[81] Xu Q, Zhong C. A general approach for estimating framework charges in metal−organic frameworks. The Journal of Physical Chemistry C. 2010;114:5035-5042.
[82] Zheng C, Zhong C. Estimation of framework charges in covalent organic frameworks using connectivity-based atom contribution method. The Journal of Physical Chemistry C. 2010;114:9945-9951.

[83] Campaná C, Mussard B, Woo TK. Electrostatic potential derived atomic charges for periodic systems using a modified error functional. Journal of Chemical Theory and Computation. 2009;5:2866-2878.
[84] Manz TA, Sholl DS. Chemically meaningful atomic charges that reproduce the electrostatic potential in periodic and nonperiodic materials. Journal of Chemical Theory and Computation. 2010;6:2455-2468.
[85] Watanabe T, Manz TA, Sholl DS. Accurate treatment of electrostatics during molecular adsorption in nanoporous crystals without assigning point charges to framework atoms. The Journal of Physical Chemistry C. 2011;115:4824-4836.
[86] Sholl DS. Understanding macroscopic diffusion of adsorbed molecules in crystalline nanoporous materials via atomistic simulations. Accounts of Chemical Research. 2006;39:403-411.
[87] Alter H. A critical investigation of polyethylene gas permeability. Journal of Polymer Science. 1962;57:925-935.
[88] Düren T, Sarkisov L, Yaghi OM, Snurr RQ. Design of new materials for methane storage. Langmuir. 2004;20:2683-2689.
[89] Brunauer S, Emmett PH, Teller E. Adsorption of Gases in Multimolecular Layers. Journal of the American Chemical Society. 1938;60:309-319.
[90] Walton KS, Snurr RQ. Applicability of the BET Method for Determining Surface Areas of Microporous Metal−Organic Frameworks. Journal of the American Chemical Society. 2007;129:8552-8556.
[91] Sarkisov L, Harrison A. Computational structure characterisation tools in application to ordered and disordered porous materials. Molecular Simulation. 2011;37:1248-1257.
[92] Myers A, Monson P. Adsorption in porous materials at high pressure: theory and experiment. Langmuir. 2002;18:10261-10273.
[93] Foster MD, Rivin I, Treacy MMJ, Delgado Friedrichs O. A geometric solution to the largest-free-sphere problem in zeolite frameworks. Microporous and Mesoporous Materials. 2006;90:32-38.
[94] Erucar I, Keskin S. Screening metal-organic framework-based mixed-matrix membranes for CO_2/CH_4 separations. Industrial and Engineering Chemistry Research. 2011;50:12606-12616.
[95] Maxwell JC. A treatise on electricity and magnetism. New York: Dover Publications; 1954.
[96] Moore TT, Mahajan R, Vu DQ, Koros WJ. Hybrid membrane materials comprising organic polymers with rigid dispersed phases. AIChE Journal. 2004;50:311-321.
[97] Battisti A, Taioli S, Garberoglio G. Zeolitic imidazolate frameworks for separation of binary mixtures of CO_2, CH_4, N_2 and H_2: a computer simulation investigation. Microporous and Mesoporous Materials. 2011;143:46-53.
[98] Bux H, Chmelik C, van Baten JM, Krishna R, Caro J. Novel MOF-membrane for molecular sieving predicted by IR-diffusion studies and molecular modeling. Advanced Materials. 2010;22:4741-4743.

[99] Haldoupis E, Watanabe T, Nair S, Sholl DS. Quantifying large effects of framework flexibility on diffusion in MOFs: CH_4 and CO_2 in ZIF-8. ChemPhysChem. 2012;13:3449-3452.
[100] Hertäg L, Bux H, Caro J, Chmelik C, Remsungnen T, Knauth M, Fritzsche S. Diffusion of CH_4 and H_2 in ZIF-8. Journal of Membrane Science. 2011;377:36-41.
[101] Keskin S, van Heest TM, Sholl DS. Can Metal–Organic Framework Materials Play a Useful Role in Large-Scale Carbon Dioxide Separations? ChemSusChem. 2010;3:879-891.
[102] Ding L, Yazaydin AOzr. How well do metal–organic frameworks tolerate flue gas impurities? The Journal of Physical Chemistry C. 2012;116:22987-22991.

APPENDIX

Appendix-A : AARE% values for Maxwell and modified Maxwell model with two different ϕ_s values

Table A.1. Calculated AARE% values for Maxwell and modified Maxwell model with two different ϕ_s values

MMM	ϕ	*AARE% CO_2*	*AARE% N_2*	*Model*	*Experimental Reference*
Cd-6F/6FDA-ODA	0.07	32.63	35.72	Maxwell	Lin et al. (2014)
ϕ_s = 0.68		41.50	44.18	Modified Maxwell	
ϕ_s = 0.75		40.11	42.85	Modified Maxwell	
ZIF-71/6FDA-Durene Pristine	0.13	34.80	22.07	Maxwell	Japip et al. (2014)
ϕ_s = 0.68		43.58	38.97	Modified Maxwell	
ϕ_s = 0.75		42.07	36.41	Modified Maxwell	
ZIF-8/6FDA-Durene (2 bar)	0.07	2.81	18.26	Maxwell	Nafisi et al. (2014)
	0.09	3.05	22.62		
	0.13	6.64	30.44		
	0.20	20.27	35.85		
	0.25	29.97	39.83		
	0.37	57.72	40.95		
ϕ_s = 0.68	0.07	8.35	22.06	Modified Maxwell	
	0.09	11.00	27.21		
	0.13	13.43	36.28		
	0.20	11.61	43.74		
	0.25	11.81	49.06		
	0.37	10.38	53.70		
ϕ_s = 0.75	0.07	6.53	21.34	Modified Maxwell	
	0.09	8.73	26.34		
	0.13	10.25	35.19		
	0.20	6.74	42.28		
	0.25	5.65	47.37		
	0.37	1.16	51.42		
ZIF-8/6FDA-Durene (6bar)	0.07	0.53	19.30	Maxwell	
	0.09	0.68	28.63		
	0.13	1.46	34.14		
	0.20	9.16	39.09		
	0.25	16.65	42.27		
	0.37	36.99	43.95		
ϕ_s = 0.68	0.07	9.35	22.98	Modified Maxwell	

	0.09	12.96	32.78		
	0.13	15.93	39.58		
	0.20	17.33	46.45		
	0.25	17.80	50.97		
	0.37	17.63	55.86		
	0.07	7.70	22.28		
	0.09	10.92	32.00		
	0.13	13.10	38.56		
$\phi_s = 0.75$	0.20	13.16	45.09	Modified Maxwell	
	0.25	12.54	49.37		
	0.37	9.87	53.72		
CuBTC/Ultem		4.08	4.08	Maxwell	
$\phi_s = 0.68$	0.44	57.02	57.02	Modified Maxwell	Duan et al. (2014)
$\phi_s = 0.75$		51.00	51.00	Modified Maxwell	
CuTPA/PVAc		11.40	30.65	Maxwell	
$\phi_s = 0.68$	0.14	14.38	0.42	Modified Maxwell	Adams et al. (2010)
$\phi_s = 0.75$		10.50	4.96	Modified Maxwell	

Appendix-B : Permeability and selectivity data of 200 new PCN-based MMMs

Table B1. Permeability and selectivity data for Matrimid-based MMMs

Matrimid (ϕ =0.3)	P_{CO_2} **(Barrer)**	P_{N_2} **(Barrer)**	S_{CO_2/N_2}
PCN-6	20.57	0.57	36.00
PCN-9-Fe	20.55	0.57	35.96
PCN-9-Co	20.57	0.57	35.99
PCN-9-Mn	20.57	0.57	35.99
PCN-10	20.57	0.57	36.00
PCN-11	20.57	0.57	36.00
PCN-26	20.57	0.57	36.00
PCN-46	20.57	0.57	36.00
PCN-80	20.57	0.57	36.00
PCN-6'	20.57	0.57	36.00
PCN-13	20.57	0.57	36.00
PCN-14	20.57	0.57	36.00
PCN-16	20.57	0.57	36.00
PCN-16'	20.57	0.57	36.00
PCN-18	20.57	0.57	36.00
PCN-19	20.57	0.57	36.00
PCN-20	20.57	0.57	36.00
PCN-39	20.56	0.57	36.00
PCN-131'	20.53	0.57	36.05
PCN-224-Ni	20.57	0.57	36.00

Table B2. Permeability and selectivity data for Ultem-based MMMs

Ultem (ϕ **=0.3)**	P_{CO_2} **(Barrer)**	P_{N_2} **(Barrer)**	S_{CO_2/N_2}
PCN-6	3.20	0.13	25.00
PCN-9-Fe	3.20	0.13	25.00
PCN-9-Co	3.20	0.13	25.00
PCN-9-Mn	3.20	0.13	25.00
PCN-10	3.20	0.13	25.00
PCN-11	3.20	0.13	25.00
PCN-26	3.20	0.13	25.00
PCN-46	3.20	0.13	25.00
PCN-80	3.20	0.13	25.00
PCN-6'	3.20	0.13	25.00
PCN-13	3.20	0.13	25.00
PCN-14	3.20	0.13	25.00
PCN-16	3.20	0.13	25.00
PCN-16'	3.20	0.13	25.00
PCN-18	3.20	0.13	25.00
PCN-19	3.20	0.13	25.00
PCN-20	3.20	0.13	25.00
PCN-39	3.20	0.13	25.00
PCN-131'	3.20	0.13	25.01
PCN-224-Ni	3.20	0.13	25.00

Table B3. Permeability and selectivity data for 6-FDA-DAM-based MMMs

6-FDA-DAM (ϕ =0.3)	P_{CO_2} **(Barrer)**	P_{N_2} **(Barrer)**	S_{CO_2/N_2}
PCN-6	1913.29	125.56	15.24
PCN-9-Fe	1761.82	125.24	14.07
PCN-9-Co	1897.04	125.51	15.11
PCN-9-Mn	1887.05	125.50	15.04
PCN-10	1905.23	121.77	15.65
PCN-11	1919.70	124.61	15.41
PCN-26	1914.78	125.58	15.25
PCN-46	1920.70	125.63	15.29
PCN-80	1914.44	125.61	15.24
PCN-6'	1913.53	125.62	15.23
PCN-13	1917.09	125.64	15.26
PCN-14	1921.37	125.58	15.30
PCN-16	1917.44	125.47	15.28
PCN-16'	1921.49	125.67	15.29
PCN-18	1919.53	125.41	15.31
PCN-19	1919.91	125.61	15.28
PCN-20	1914.60	125.55	15.25
PCN-39	1869.14	125.44	14.90
PCN-131'	1631.60	78.67	20.74
PCN-224-Ni	1914.27	125.58	15.24

Table B4. Permeability and selectivity data for Polyimide-based MMMs

Polyimide (ϕ =0.3)	P_{CO_2} **(Barrer)**	P_{N_2} **(Barrer)**	S_{CO_2/N_2}
PCN-6	102.82	2.90	35.42
PCN-9-Fe	102.33	2.90	35.26
PCN-9-Co	102.77	2.90	35.41
PCN-9-Mn	102.74	2.90	35.40
PCN-10	102.80	2.90	35.44
PCN-11	102.84	2.90	35.43
PCN-26	102.83	2.90	35.42
PCN-46	102.84	2.90	35.43
PCN-80	102.82	2.90	35.42
PCN-6'	102.82	2.90	35.42
PCN-13	102.83	2.90	35.43
PCN-14	102.85	2.90	35.43
PCN-16	102.83	2.90	35.43
PCN-16'	102.85	2.90	35.43
PCN-18	102.84	2.90	35.43
PCN-19	102.84	2.90	35.43
PCN-20	102.83	2.90	35.42
PCN-39	102.69	2.90	35.38
PCN-131'	101.81	2.85	35.69
PCN-224-Ni	102.82	2.90	35.42

Table B5. Permeability and selectivity data for MEEP-based MMMs

MEEP (ϕ **=0.3)**	P_{CO_2} **(Barrer)**	P_{N_2} **(Barrer)**	S_{CO_2/N_2}
PCN-6	570.35	9.14	62.39
PCN-9-Fe	555.73	9.14	60.80
PCN-9-Co	568.89	9.14	62.23
PCN-9-Mn	567.98	9.14	62.13
PCN-10	569.62	9.12	62.45
PCN-11	570.92	9.14	62.48
PCN-26	570.48	9.14	62.40
PCN-46	571.00	9.14	62.46
PCN-80	570.44	9.14	62.40
PCN-6'	570.37	9.14	62.39
PCN-13	570.68	9.14	62.42
PCN-14	571.06	9.14	62.46
PCN-16	570.71	9.14	62.43
PCN-16'	571.07	9.14	62.46
PCN-18	570.90	9.14	62.45
PCN-19	570.93	9.14	62.45
PCN-20	570.46	9.14	62.40
PCN-39	566.32	9.14	61.95
PCN-131'	541.11	8.67	62.41
PCN-224-Ni	570.43	9.14	62.40

Table B6. Permeability and selectivity data for PIM-1-based MMMs

PIM-1 (ϕ =0.3)	P_{CO_2} **(Barrer)**	P_{N_2} **(Barrer)**	S_{CO_2/N_2}
PCN-6	5167.38	209.92	24.62
PCN-9-Fe	4240.75	209.04	20.29
PCN-9-Co	5052.11	209.77	24.08
PCN-9-Mn	4983.35	209.76	23.76
PCN-10	5109.64	199.61	25.60
PCN-11	5214.14	207.27	25.16
PCN-26	5178.22	209.97	24.66
PCN-46	5221.51	210.12	24.85
PCN-80	5175.74	210.05	24.64
PCN-6'	5169.13	210.09	24.60
PCN-13	5195.05	210.15	24.72
PCN-14	5226.42	209.98	24.89
PCN-16	5197.56	209.68	24.79
PCN-16'	5227.36	210.23	24.87
PCN-18	5212.93	209.49	24.88
PCN-19	5215.69	210.06	24.83
PCN-20	5176.87	209.90	24.66
PCN-39	4864.11	209.58	23.21
PCN-131'	3646.16	112.29	32.47
PCN-224-Ni	5174.50	209.98	24.64

Table B7. Permeability and selectivity data for PIM-7-based MMMs

PIM-7 (ϕ =0.3)	P_{CO_2} **(Barrer)**	P_{N_2} **(Barrer)**	S_{CO_2/N_2} **Selectivity**
PCN-6	2493.50	95.92	25.99
PCN-9-Fe	2244.75	95.74	23.45
PCN-9-Co	2466.05	95.89	25.72
PCN-9-Mn	2449.25	95.89	25.54
PCN-10	2479.86	93.69	26.47
PCN-11	2504.39	95.36	26.26
PCN-26	2496.04	95.93	26.02
PCN-46	2506.09	95.97	26.11
PCN-80	2495.46	95.95	26.01
PCN-6'	2493.91	95.96	25.99
PCN-13	2499.96	95.97	26.05
PCN-14	2507.23	95.94	26.13
PCN-16	2500.55	95.87	26.08
PCN-16'	2507.45	95.99	26.12
PCN-18	2504.11	95.83	26.13
PCN-19	2504.75	95.95	26.10
PCN-20	2495.72	95.92	26.02
PCN-39	2419.34	95.85	25.24
PCN-131'	2043.13	64.81	31.52
PCN-224-Ni	2495.17	95.94	26.01

Table B8. Permeability and selectivity data for modified PDMS-based MMMs

modified PDMS (ϕ =0.3)	P_{CO_2} **(Barrer)**	P_{N_2} **(Barrer)**	S_{CO_2/N_2}
PCN-6	4503.35	133.56	33.72
PCN-9-Fe	3775.53	133.21	28.34
PCN-9-Co	4415.31	133.51	33.07
PCN-9-Mn	4362.47	133.50	32.68
PCN-10	4459.34	129.29	34.49
PCN-11	4538.87	132.49	34.26
PCN-26	4511.59	133.59	33.77
PCN-46	4544.45	133.65	34.00
PCN-80	4509.70	133.62	33.75
PCN-6'	4504.68	133.63	33.71
PCN-13	4524.38	133.66	33.85
PCN-14	4548.18	133.59	34.05
PCN-16	4526.29	133.47	33.91
PCN-16'	4548.89	133.69	34.03
PCN-18	4537.95	133.39	34.02
PCN-19	4540.04	133.62	33.98
PCN-20	4510.57	133.56	33.77
PCN-39	4270.23	133.43	32.00
PCN-131'	3283.11	82.17	39.95
PCN-224-Ni	4508.77	133.59	33.75

Table B9. Permeability and selectivity data for PTMGP-based MMMs

PTMGP (ϕ =0.3)	P_{CO_2} **(Barrer)**	P_{N_2} **(Barrer)**	S_{CO_2/N_2}
PCN-6	29026.31	2242.95	12.94
PCN-9-Fe	15909.82	2148.90	7.40
PCN-9-Co	26020.25	2227.18	11.68
PCN-9-Mn	24546.97	2225.38	11.03
PCN-10	27424.88	1536.34	17.85
PCN-11	30492.26	1987.13	15.34
PCN-26	29351.44	2249.49	13.05
PCN-46	30738.87	2266.77	13.56
PCN-80	29276.26	2258.34	12.96
PCN-6'	29078.24	2262.48	12.85
PCN-13	29873.39	2270.01	13.16
PCN-14	30906.18	2250.03	13.74
PCN-16	29953.37	2216.28	13.52
PCN-16'	30938.39	2279.07	13.57
PCN-18	30452.06	2195.94	13.87
PCN-19	30543.80	2259.93	13.52
PCN-20	29310.62	2241.10	13.08
PCN-39	22409.11	2205.40	10.16
PCN-131'	12897.37	692.87	18.61
PCN-224-Ni	29239.04	2250.44	12.99

Table B10. Permeability and selectivity data for PTMSP-based MMMs

PTMSP (ϕ =0.3)	P_{CO_2} **(Barrer)**	P_{N_2} **(Barrer)**	S_{CO_2/N_2}
PCN-6	55050.79	5872.62	9.37
PCN-9-Fe	26476.54	5295.50	5.00
PCN-9-Co	46128.36	5768.61	8.00
PCN-9-Mn	42422.46	5756.94	7.37
PCN-10	50045.46	3066.86	16.32
PCN-11	60232.77	4500.48	13.38
PCN-26	56146.72	5916.71	9.49
PCN-46	61168.91	6035.94	10.13
PCN-80	55890.71	5977.25	9.35
PCN-6'	55223.89	6005.95	9.19
PCN-13	57968.05	6058.75	9.57
PCN-14	61815.47	5920.37	10.44
PCN-16	58254.12	5698.56	10.22
PCN-16'	61941.02	6123.35	10.12
PCN-18	60082.01	5571.55	10.78
PCN-19	60426.78	5988.27	10.09
PCN-20	56007.53	5860.29	9.56
PCN-39	37661.28	5630.05	6.69
PCN-131'	22494.61	1730.40	13.00
PCN-224-Ni	55764.57	5923.15	9.41

Appendix-C: Change in MMM permeability and selectivity when the filler flexibility is considered for PCN-10, PCN-11 and PCN-9-Fe

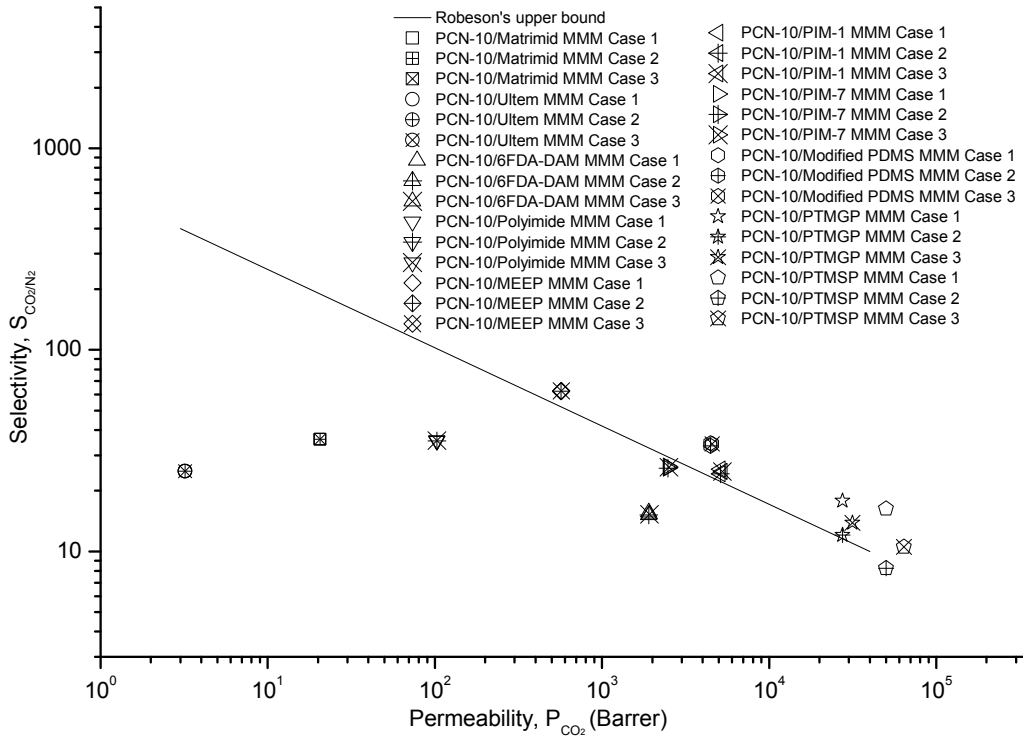

Figure C1. Change in CO_2 permeability and selectivity of PCN-10-based MMMs when flexibility of the filler was considered.

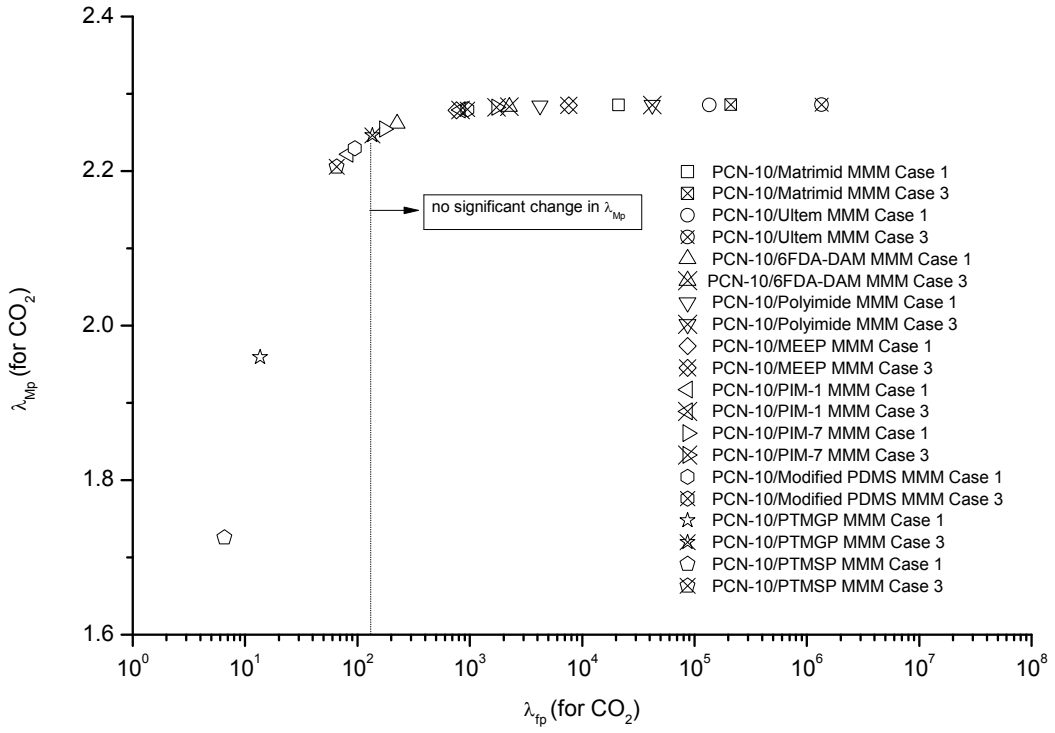

Figure C2. Change in CO_2 permeability of MMM vs. change in CO_2 permeability of filler (PCN-10). CO_2 permeability is same for Case 1 and Case 2, therefore data for Case 2 is not shown.

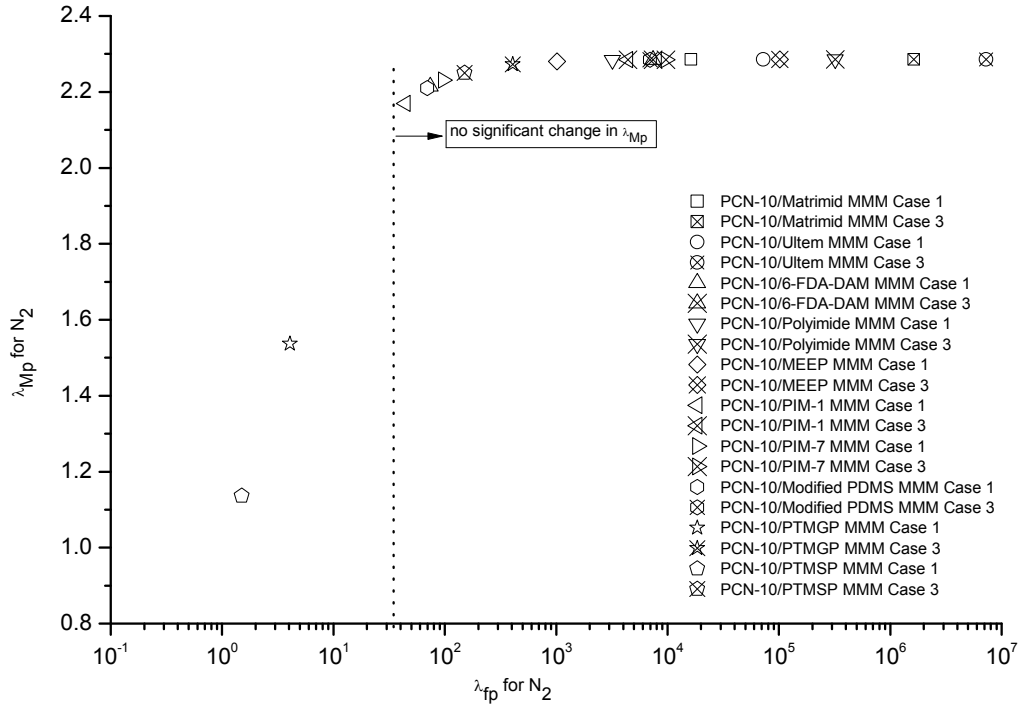

Figure C3. Change in N_2 permeability of MMM vs. change in N_2 permeability of filler (PCN-10). N_2 permeability is same for Case 2 and for Case 3, therefore data for Case 2 are not shown.

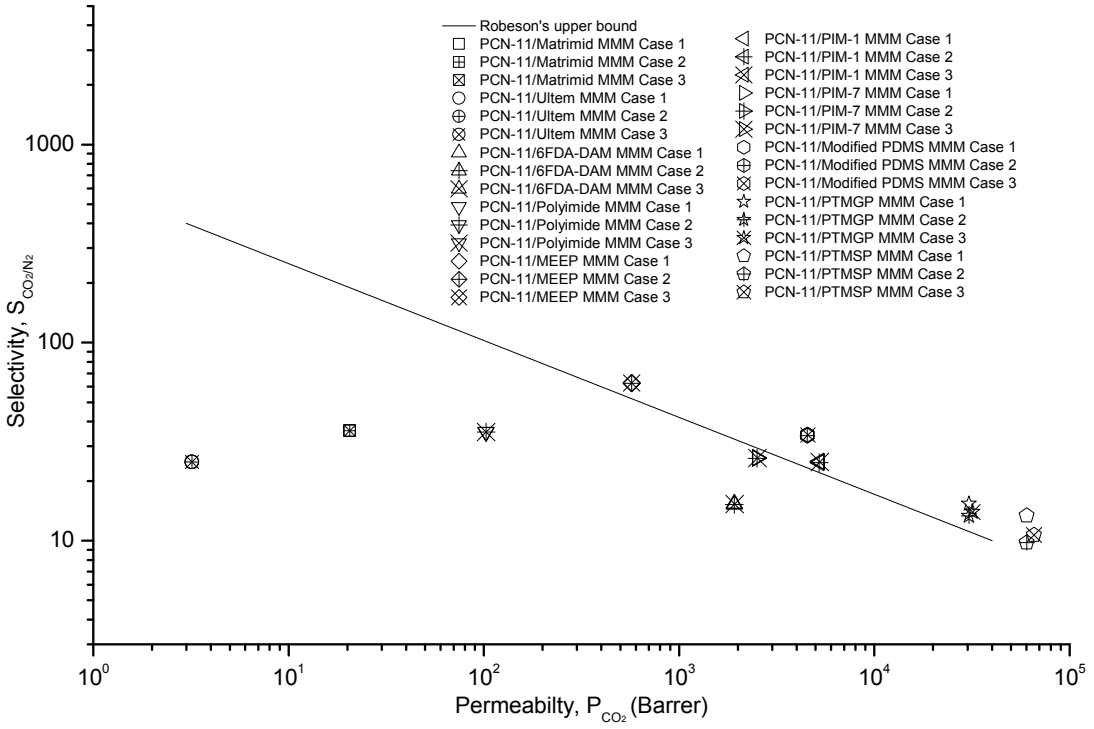

Figure C4. Change in CO_2 permeability and selectivity of PCN-11-based MMMs when flexibility of the filler was considered.

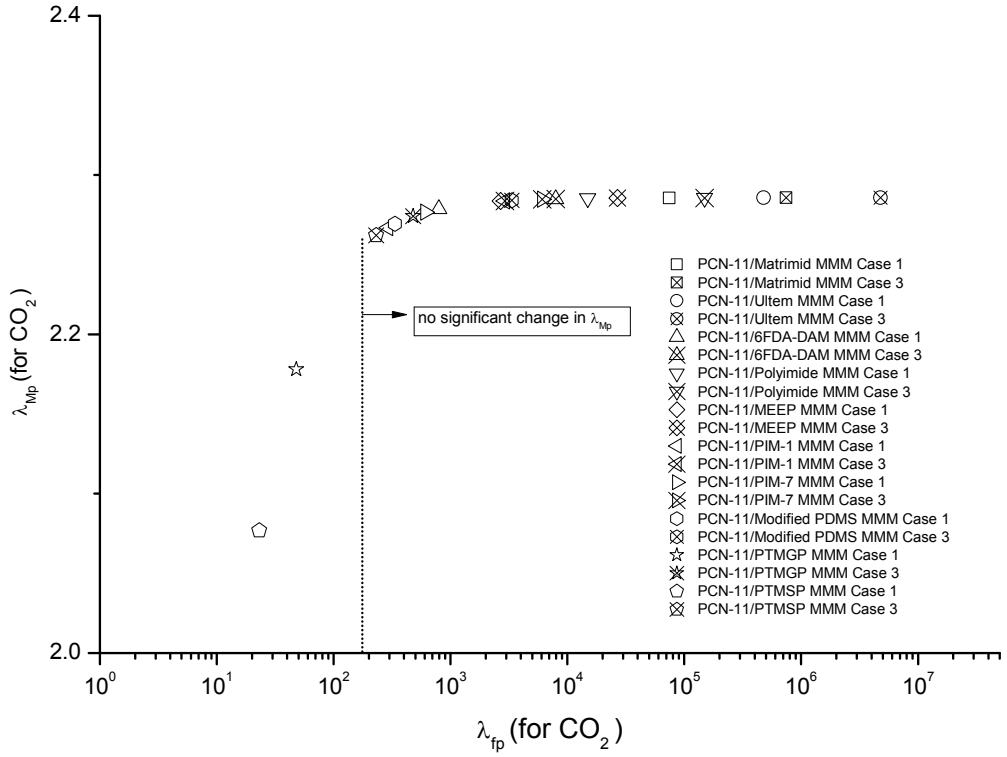

Figure C5. Change in CO_2 permeability of MMM vs. change in CO_2 permeability of filler (PCN-11). CO_2 permeability is same for Case1 and Case 2, therefore data for Case 2 is not shown.

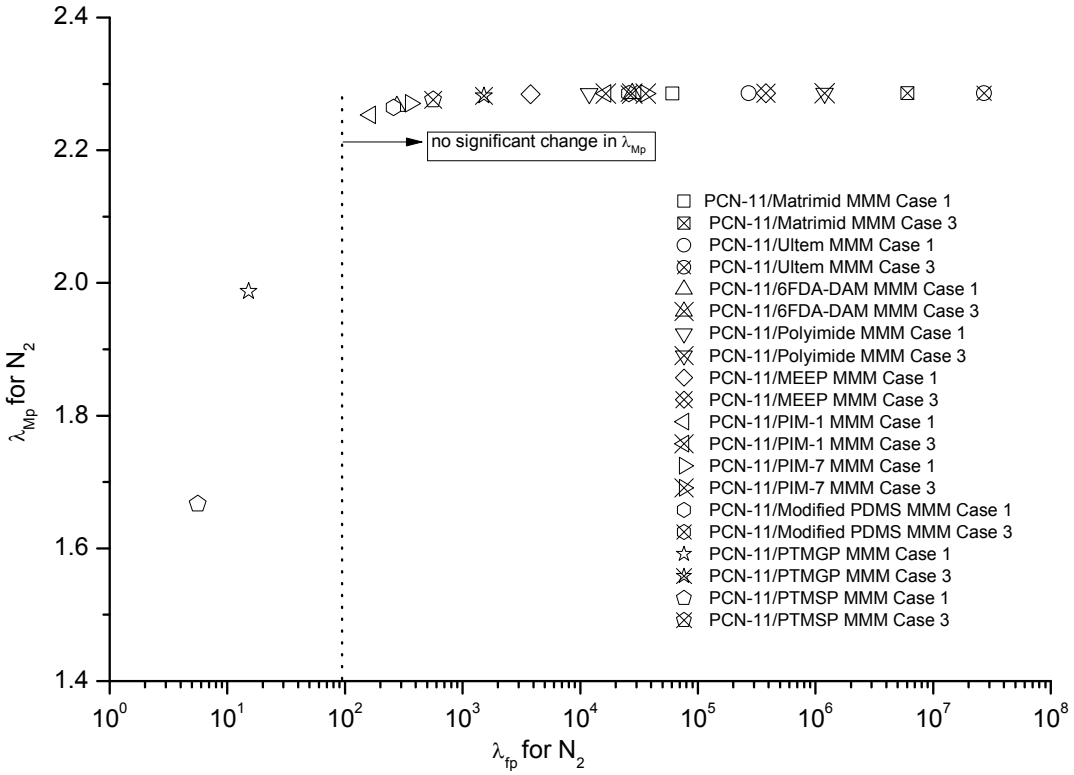

Figure C6. Change in N_2 permeability of MMM vs. change in N_2 permeability of filler (PCN-11). N_2 permeability is same for Case 2 and for Case 3, therefore data for Case 2 are not shown.

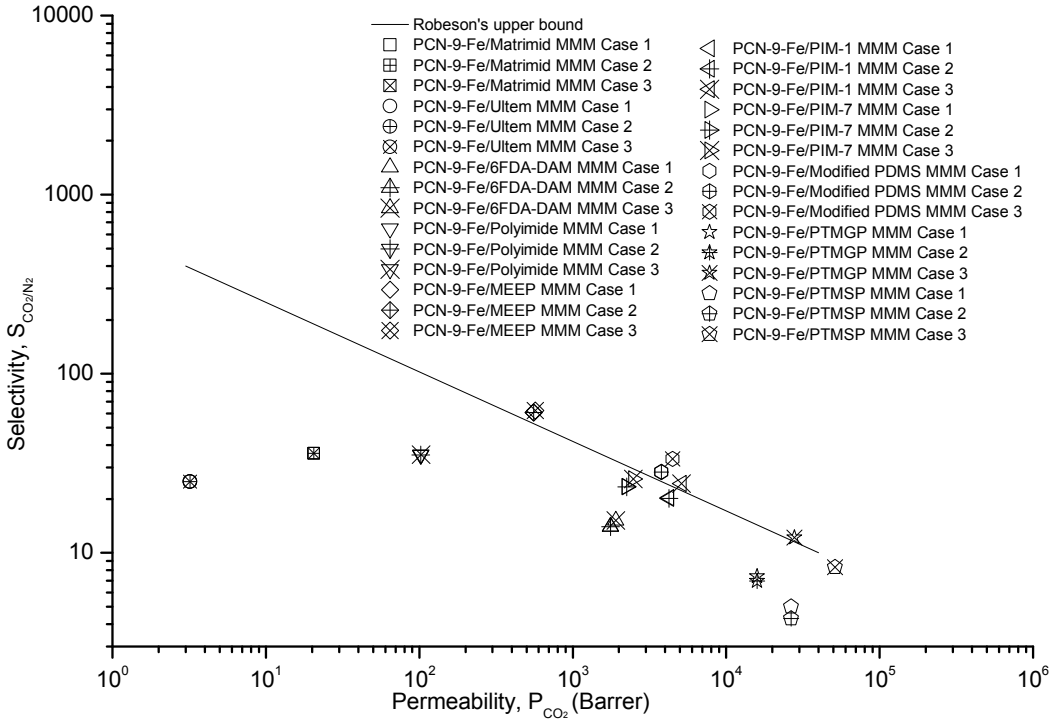

Figure C7. Change in CO_2 permeability and selectivity of PCN-9-Fe-based MMMs when flexibility of the filler was considered.

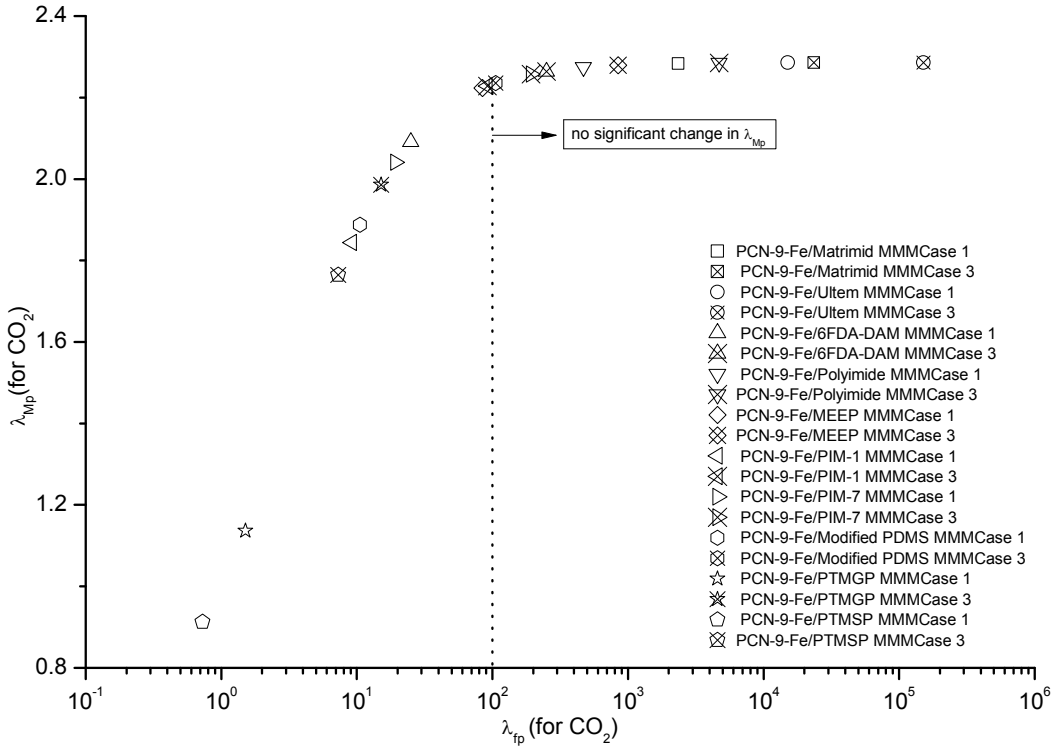

Figure C8. Change in CO_2 permeability of MMM vs. change in CO_2 permeability of filler (PCN-9-Fe). CO_2 permeability is same for Case1 and Case 2, therefore data for Case 2 is not shown.

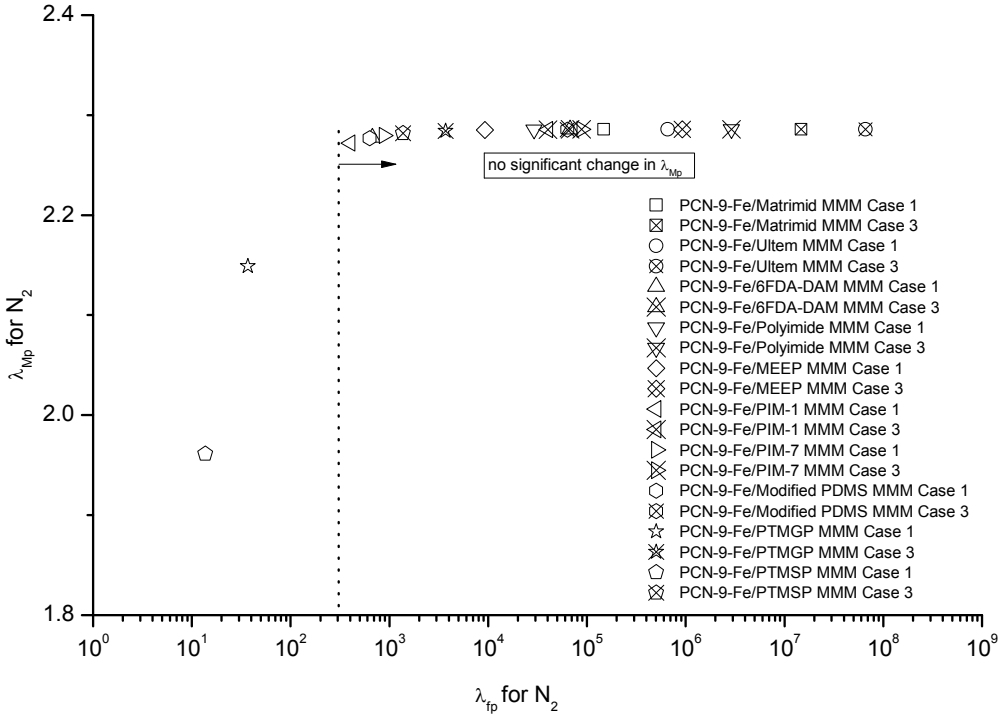

Figure C9. Change in N_2 permeability of MMM vs. change in N_2 permeability of filler (PCN-9-Fe). N_2 permeability is same for Case 2 and for Case 3; therefore data for Case 2 are not shown.

VITA

Çiğdem Altıntaş was born in İstanbul, Turkey, on 29 August 1989. In 2008, she graduated from Chemical and Biological Engineering Department of Koç University. She successfully got his MSc degree from Chemical and Biological Engineering Department at Koç University. Her research interests include molecular modelling of metal organic frameworks and theoretical calculations of mixed matrix membrane performance for gas separations. She is going to continue her PhD study in Chemical and Biological Department in Koç University.

Publications :

- Altintas, C. and Keskin, S. (2015) "Molecular simulations of porous coordination network-based mixed matrix membranes for CO_2/N_2 separations" Mol Simul. 2015:1-13.